Supplementary Information (SI) for CrystEngComm.

1D chains and an open 3D network from poly(diethylamidinium) cations and carboxylate anions

Meabh K. S. Perry-Britton, Jessica J. Du and Nicholas G. White*

Research School of Chemistry, The Australian National University, Canberra, 2601, ACT, Australia
Email: nicholas.white@anu.edu.au URL: www.nwhitegroup.com

1 Synthesis and characterisation

1.1 Details of instrumentation

NMR spectra were collected on a Bruker Avance 400 or Bruker Avance 700 spectrometer and are referenced to the residual solvent signal.[1] Infrared spectra were recorded on a Perkin-Elmer Spectrum Two FT-IR Spectrometer fitted with an ATR Two Single Reflection Diamond. Electrospray ionisation mass spectrometry data were acquired on a Waters Synapt or Orbitrap Elite spectrometer. PXRD data were recorded on a Panalytical Empyrean 2 diffractometer using Cu Kα radiation and a PIXcel detector. Details of SCXRD studies are given in Section 3 of this document.

1.2 Characterisation data for building blocks

1.2.1 Characterisation data for ^{Et}model-amide

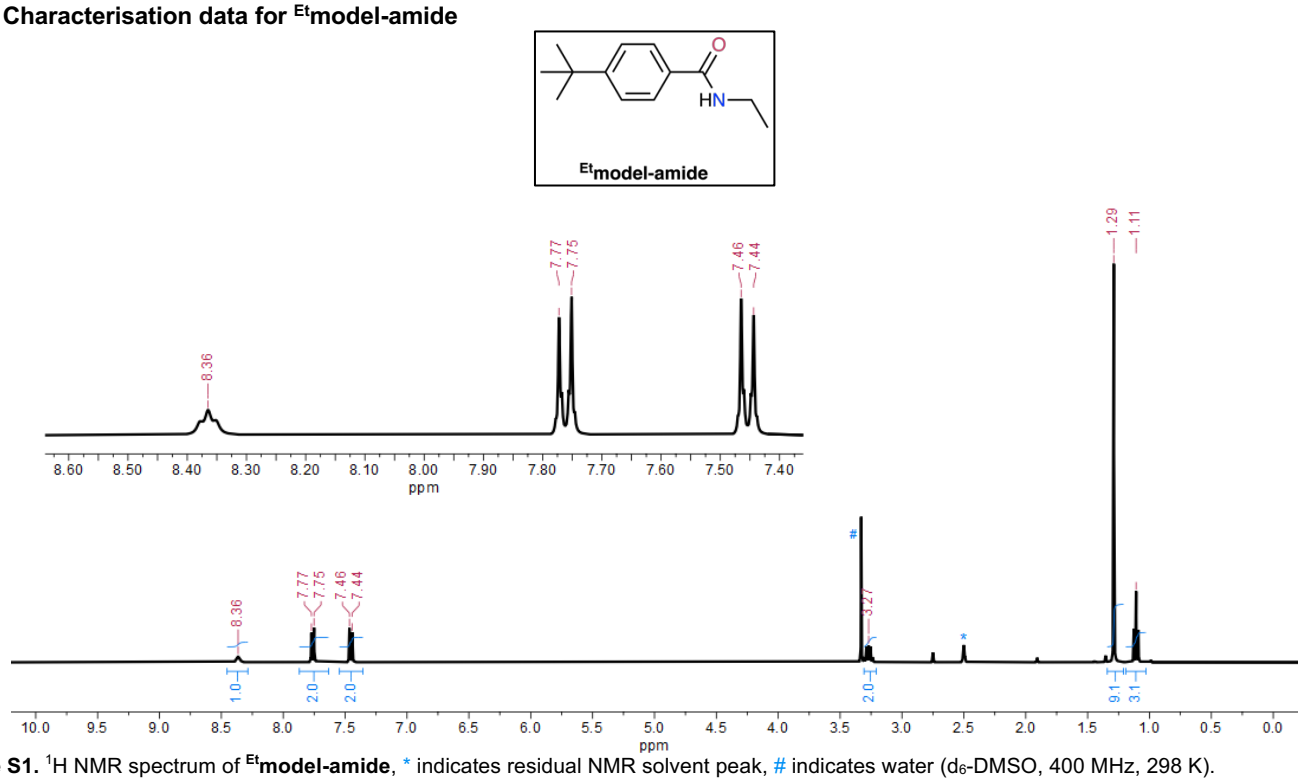

Figure S1. ^{1}H NMR spectrum of **^{Et}model-amide**, * indicates residual NMR solvent peak, # indicates water (d_6-DMSO, 400 MHz, 298 K).

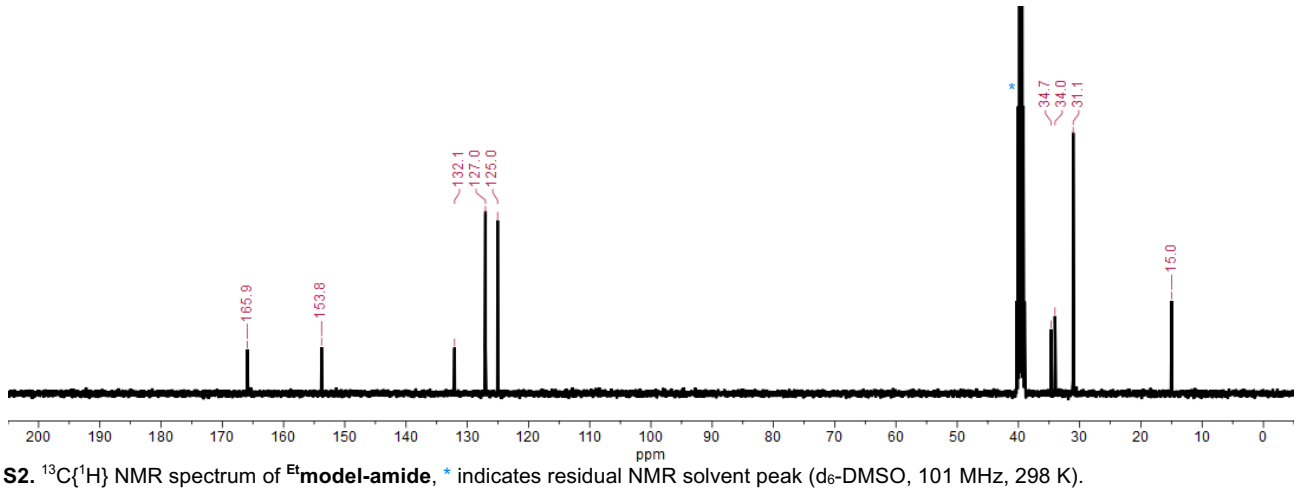

Figure S2. ^{13}C{^{1}H} NMR spectrum of **^{Et}model-amide**, * indicates residual NMR solvent peak (d_6-DMSO, 101 MHz, 298 K).

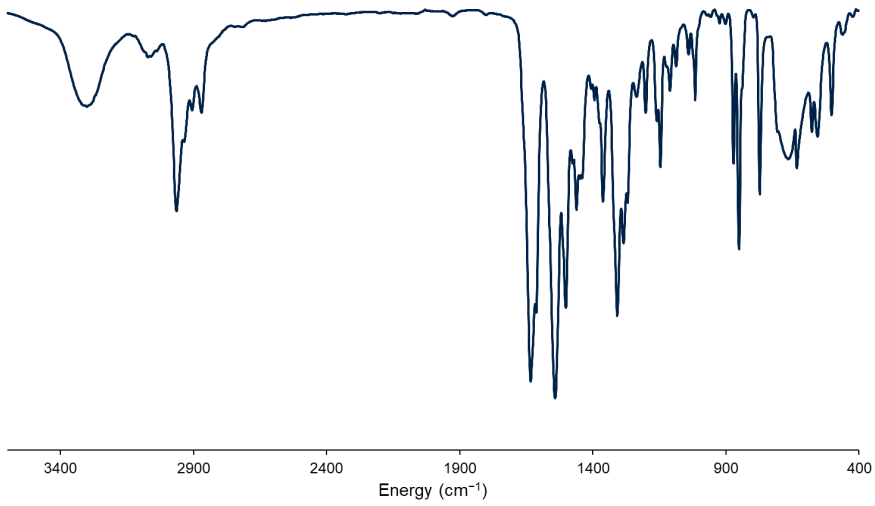

Figure S3. ATR-IR spectrum of **model-amide**.

1.2.2 Characterisation data for ^{Et}model·BPh$_4$

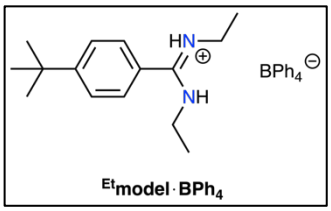

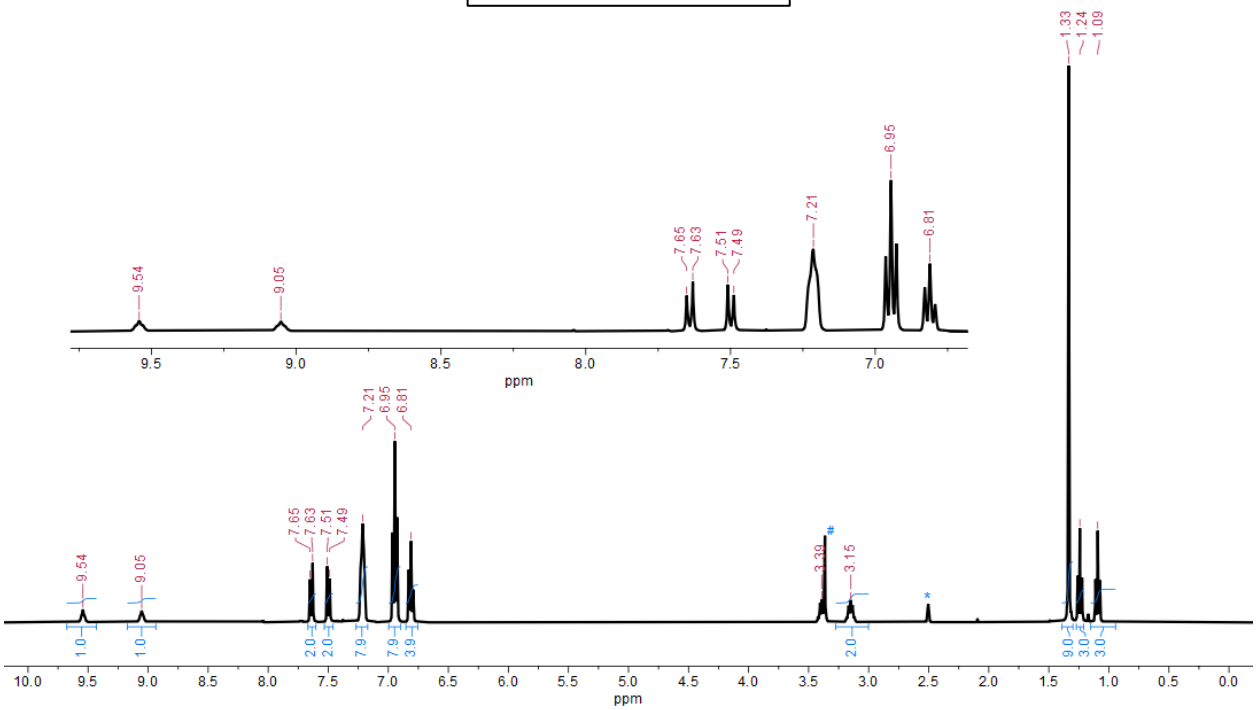

Figure S4. ^{1}H NMR spectrum of ^{Et}**model·BPh$_4$**, * indicates residual NMR solvent peak, # indicates water (d$_6$-DMSO, 400 MHz, 298 K).

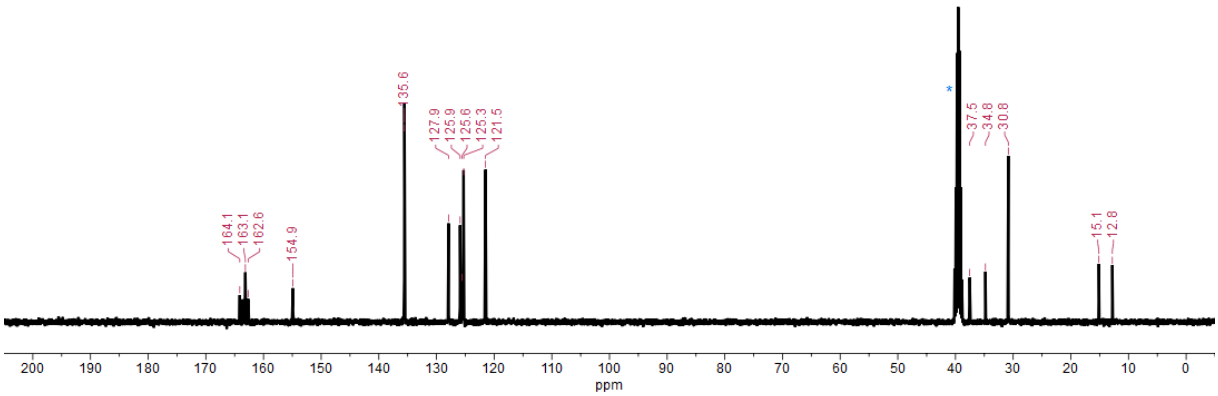

Figure S5. ^{13}C{^{1}H} NMR spectrum of ^{Et}**model·BPh$_4$**, * indicates residual NMR solvent peak (d$_6$-DMSO, 101 MHz, 298 K).

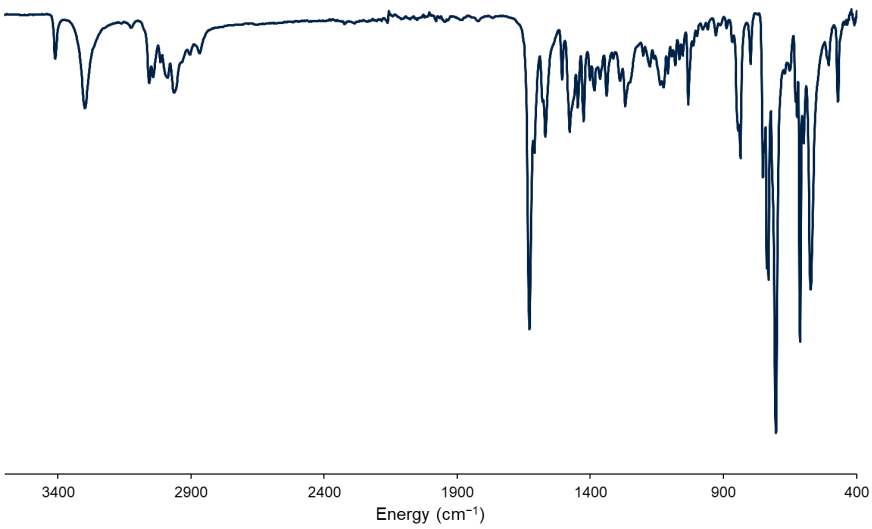

Figure S6. ATR-IR spectrum of **model·BPh$_4$**.

1.2.3 Characterisation data for ^{Et}biphen-amide

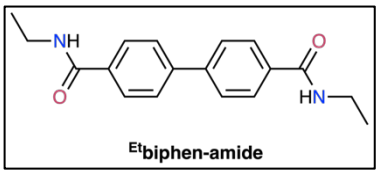

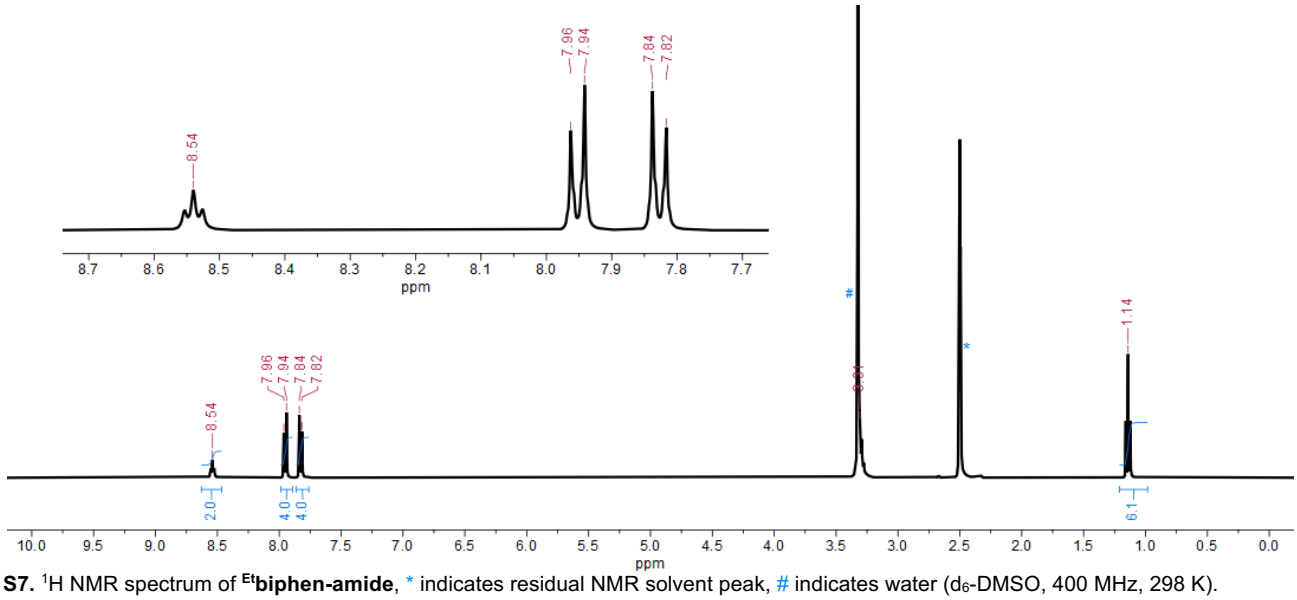

Figure S7. ^{1}H NMR spectrum of **^{Et}biphen-amide**, * indicates residual NMR solvent peak, # indicates water (d_6-DMSO, 400 MHz, 298 K).

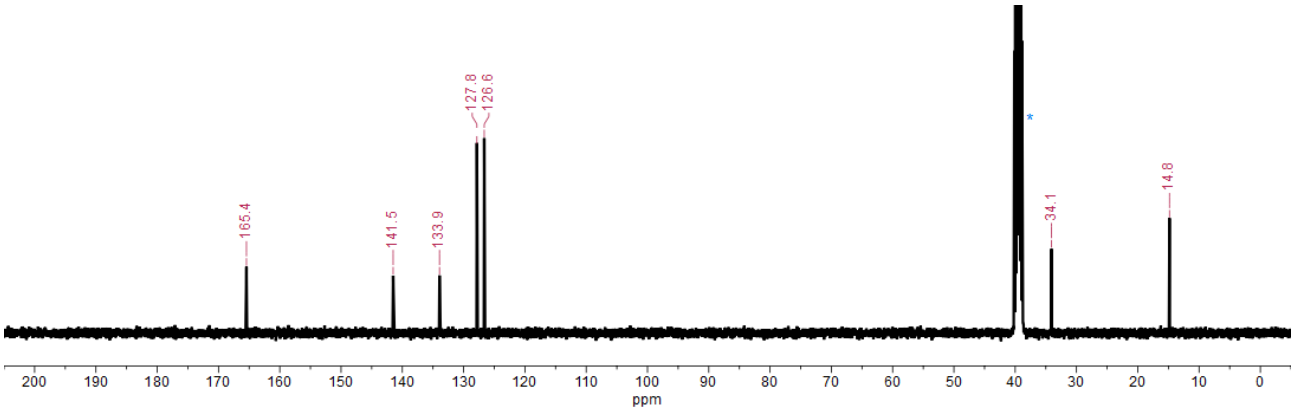

Figure S8. ^{13}C{^{1}H} NMR spectrum of **^{Et}biphen-amide**, * indicates residual NMR solvent peak (d_6-DMSO, 101 MHz, 298 K).

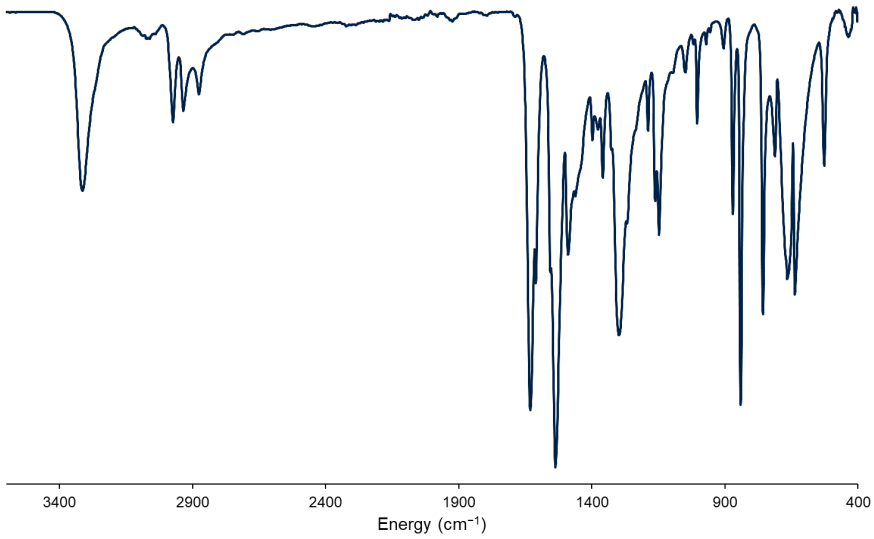

Figure S9. ATR-IR spectrum of **biphen-amide**.

1.2.4 Characterisation data for ^{Et}biphen·Cl_2

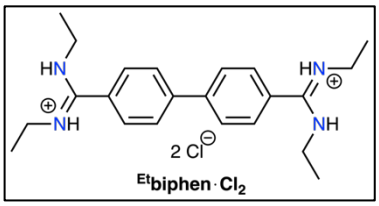

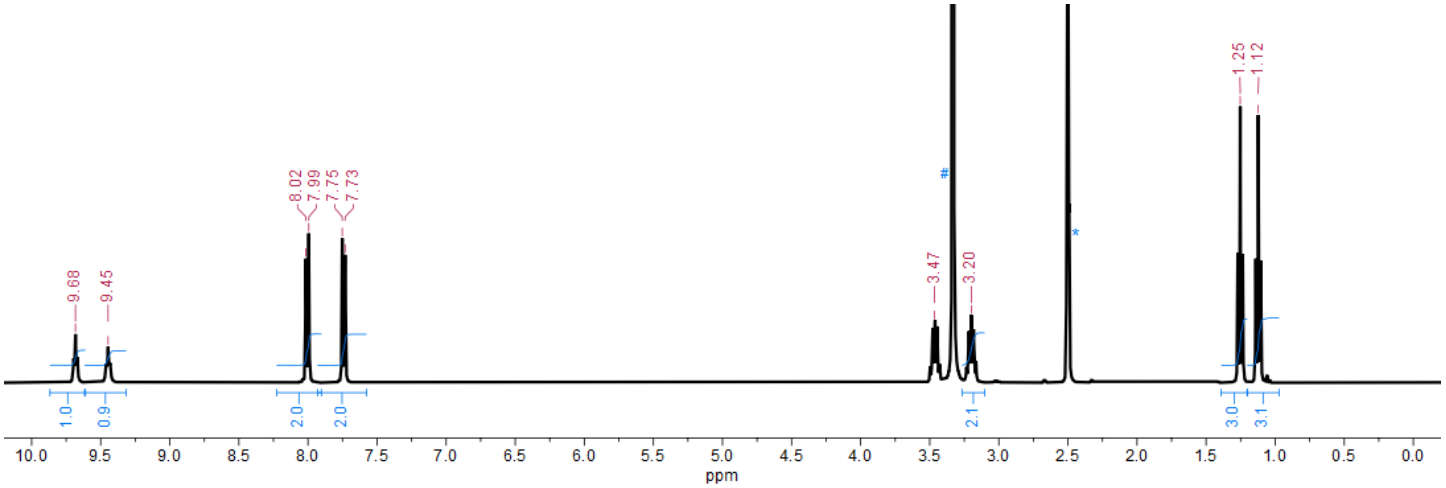

Figure S10. ^{1}H NMR spectrum of ^{Et}**biphen·Cl_2**, * indicates residual NMR solvent peak, # indicates water (d_6-DMSO, 400 MHz, 298 K).

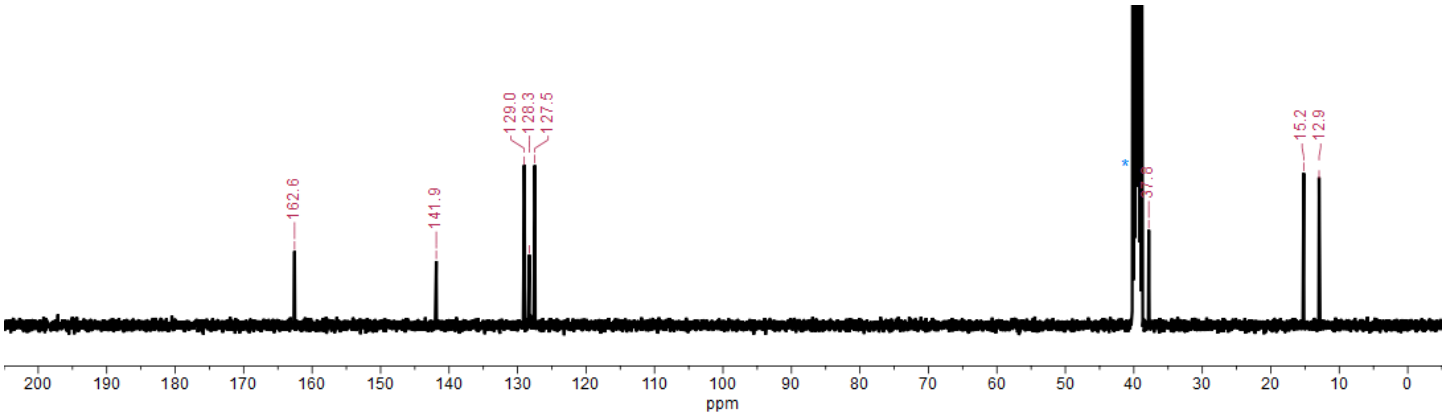

Figure S11. ^{13}C{^{1}H} NMR spectrum of ^{Et}**biphen·Cl_2**, * indicates residual NMR solvent peak (d_6-DMSO, 101 MHz, 298 K).

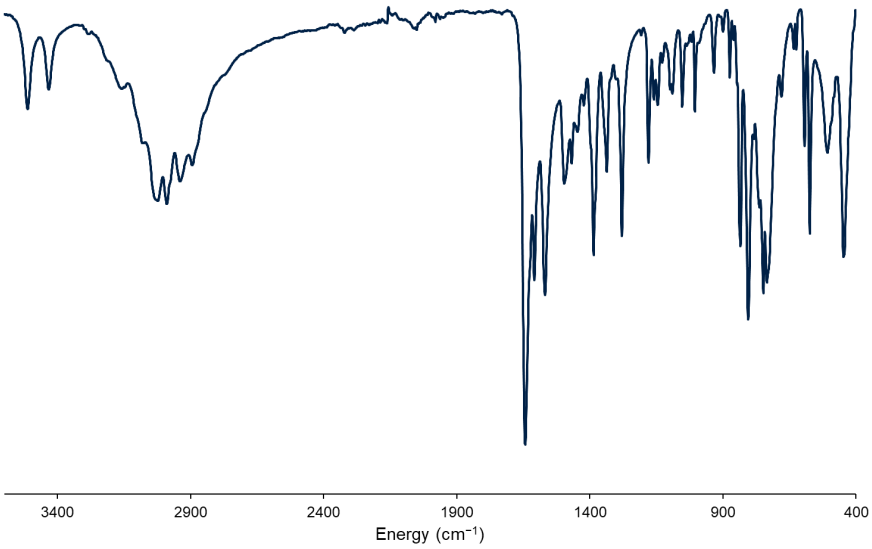

Figure S12. ATR-IR spectrum of **biphen·Cl_2**.

1.2.5 Characterisation data for ^{Et}tetra-amide

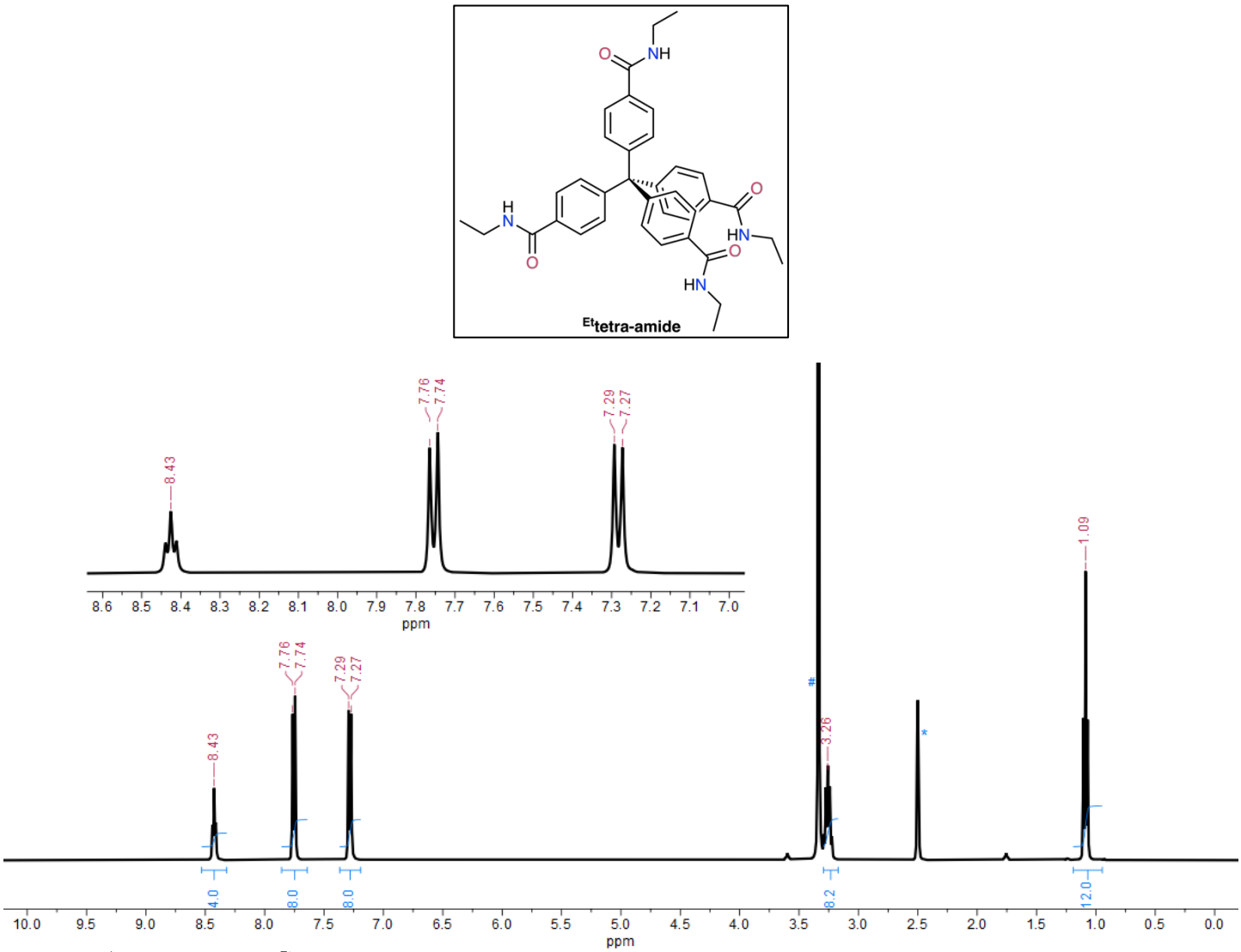

Figure S13. ^{1}H NMR spectrum of **^{Et}tetra-amide**, * indicates residual NMR solvent peak, # indicates water (d_6-DMSO, 400 MHz, 298 K).

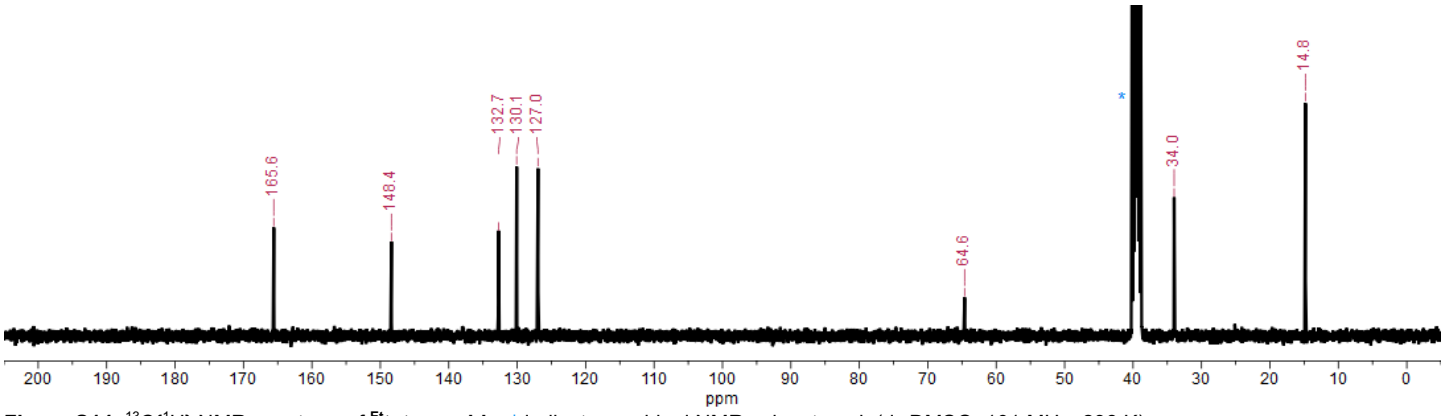

Figure S14. ^{13}C{^{1}H} NMR spectrum of **^{Et}tetra-amide**, * indicates residual NMR solvent peak (d_6-DMSO, 101 MHz, 298 K).

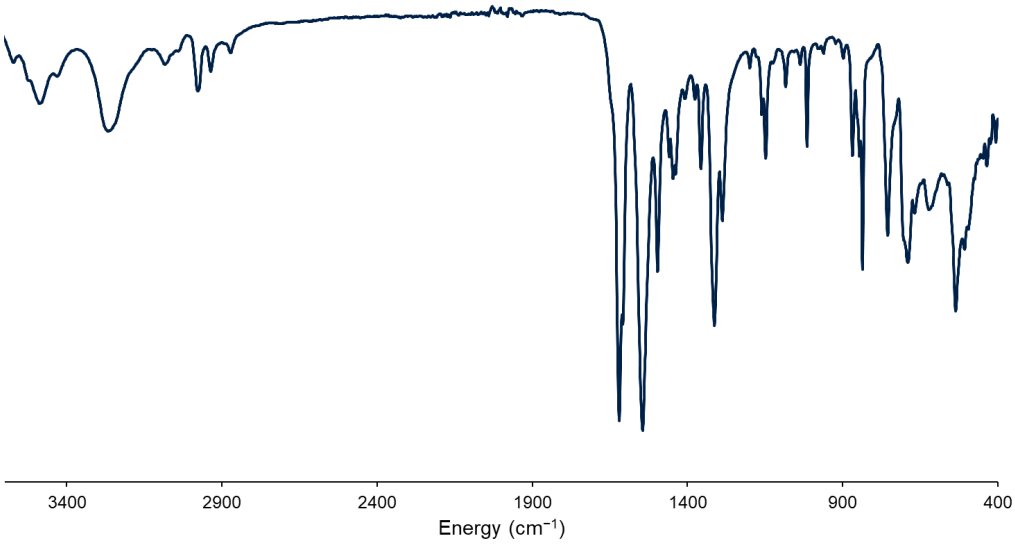

Figure S15. ATR-IR spectrum of **tetra-amide**.

1.2.6 Characterisation data for ^{Et}tetra·Cl$_4$

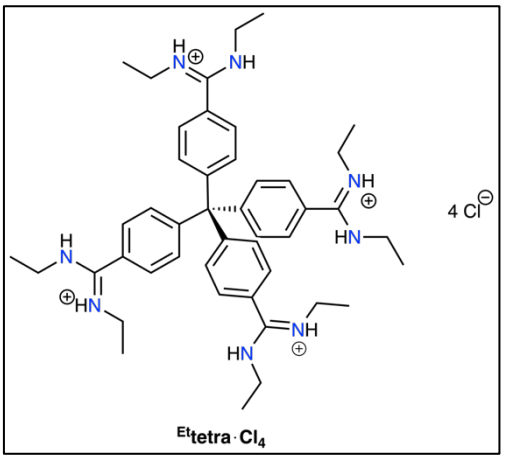

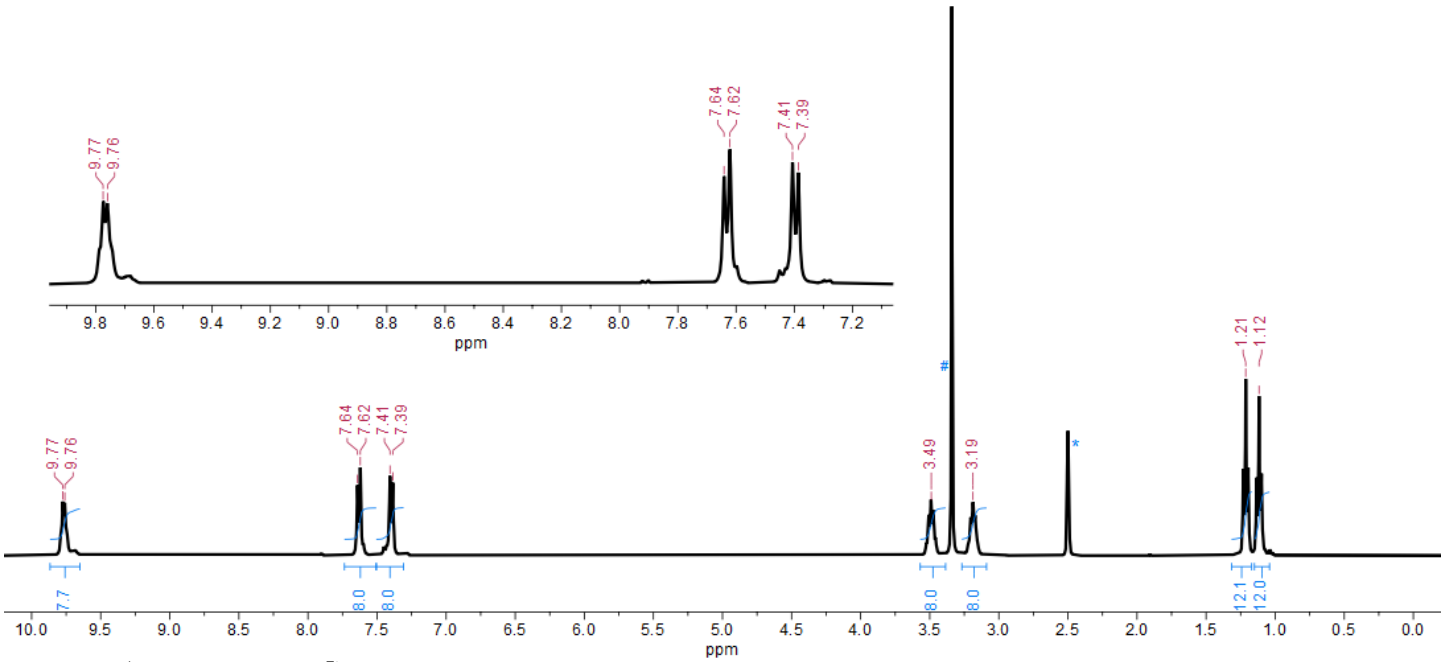

Figure S16. ^{1}H NMR spectrum of ^{Et}tetra·Cl$_4$, * indicates residual NMR solvent peak, # indicates water (d_6-DMSO, 400 MHz, 298 K).

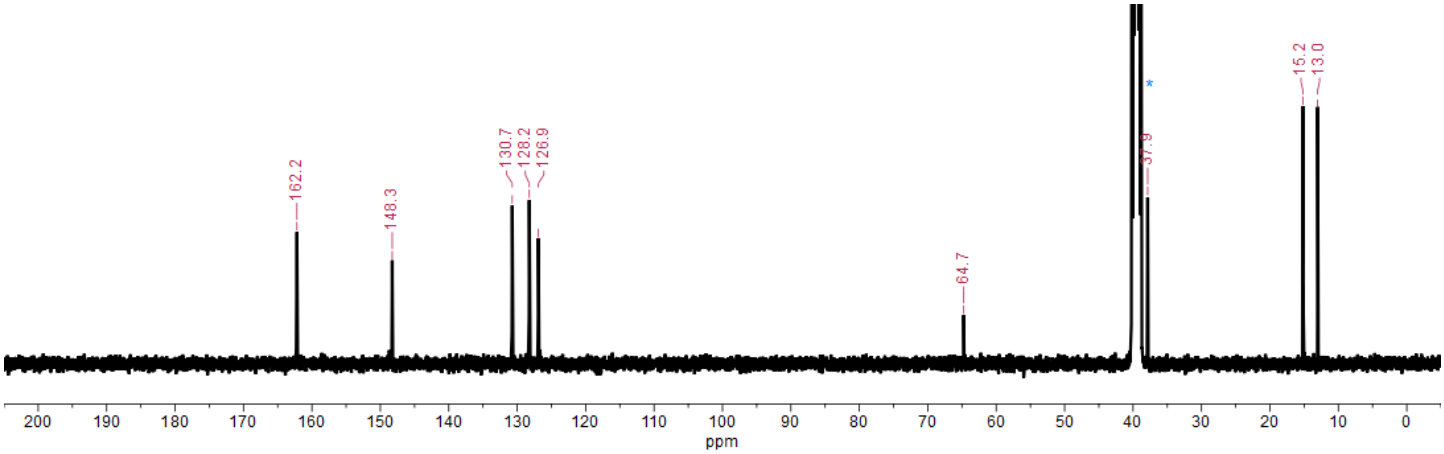

Figure S17. $^{13}C\{^{1}H\}$ NMR spectrum of ^{Et}**tetra·Cl$_4$**, * indicates residual NMR solvent peak (d_6-DMSO, 101 MHz, 298 K).

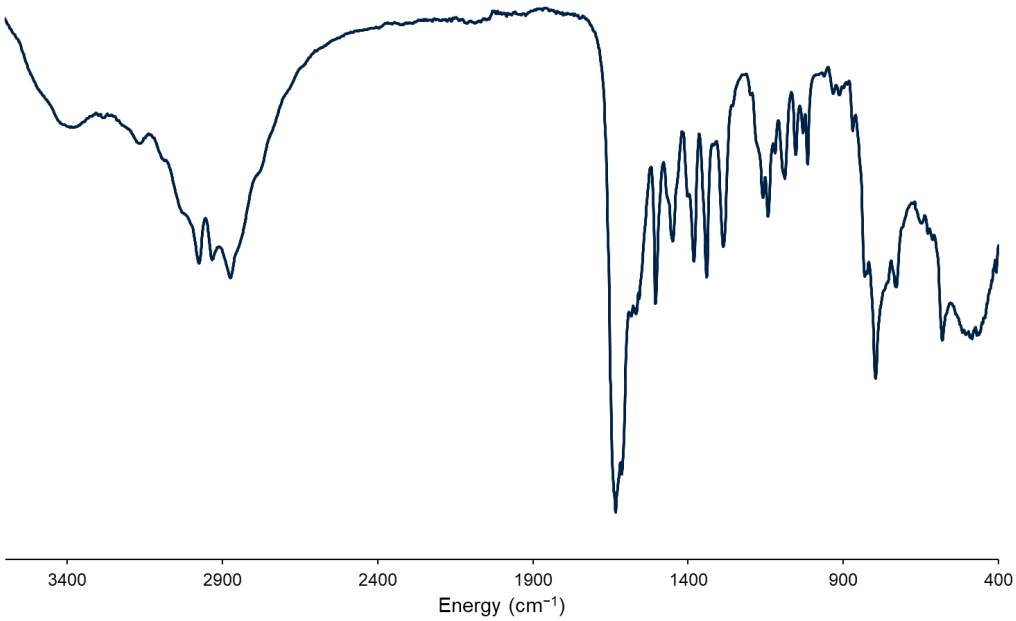

Figure S18. ATR-IR spectrum of **tetra·Cl$_4$**.

1.3 Initial crystallisation of hydrogen-bonded networks

Initially, crystallisations were completed on a small scale at room temperature (unless stated otherwise), primarily focusing on the solvents water and ethanol as these had proven most effective in our previous studies with dimethylamidinium derivatives.[2] In all crystallisations, a solution of the carboxylate component was added to a solution of the alkyl-amidinium and the mixture left to stand for at least a week. Full details are provided in Tables S1 – S6.

Table S1: Summary of **^{Et}biphen·Cl$_2$** and **TBA$_2$·TP** crystallisation conditions and outcomes.

Solvent	Conc. of ^{Et}biphen·Cl$_2$ (mM)	Conc. of TBA$_2$·TP (mM)	Molar ratio	Precipitate?	Product
H_2O	10	10	1:1	x	–
	5.0	5.0	1:1	x	–
	2.5	2.5	1:1	x	–
	1.3	1.3	1:1	x	–
	0.63	0.63	1:1	x	–
EtOH	20	20	1:1	✓	**^{Et}biphen·TP**
	10	10	1:1	✓	**^{Et}biphen·TP**
	5.0	5.0	1:1	x	–
	2.5	2.5	1:1	x	–
	1.3	1.3	1:1	x	–
	0.63	0.63	1:1	x	–

Table S2: Summary of **^{Et}biphen·Cl$_2$** and **TBA$_2$·BPDC** crystallisation conditions and outcomes.

Solvent	Conc. of ^{Et}biphen·Cl$_2$ (mM)	Conc. of TBA$_2$·BPDC (mM)	Molar ratio	Precipitate?	Product
H_2O	10	10	1:1	x	–
	5.0	5.0	1:1	x	–
	2.5	2.5	1:1	x	–
	1.3	1.3	1:1	x	–
	0.63	0.63	1:1	x	–
EtOH	20	20	1:1	✓	**^{Et}biphen·BPDC**[a]
	10	10	1:1	✓	**^{Et}biphen·BPDC**[a]
	5.0	5.0	1:1	?	amorphous solid
	2.5	2.5	1:1	x	–
	1.3	1.3	1:1	x	–
	0.63	0.63	1:1	x	–

[a] This crystallisation gave only a small number of crystals. Repeating this crystallisation several times always gave the same result, *i.e.* a small number of crystals, insufficient for bulk characterisation.

Table S3: Summary of **^{Et}biphen·Cl$_2$** and **TBA$_4$·TC** crystallisation conditions and outcomes.

Solvent	Conc. of ^{Et}biphen·Cl$_2$ (mM)	Conc. of TBA$_4$·TC (mM)	Molar ratio	Precipitate?	Product
H_2O	20	10	2:1	x	–
	10	5.0	2:1	x	–
	5.0	2.5	2:1	x	–
	2.5	1.3	2:1	x	–
	1.3	0.63	2:1	x	–
EtOH	20	10	2:1	x	–
	10	5.0	2:1	x	–
	5.0	2.5	2:1	x	–
	2.5	1.3	2:1	x	–
	1.3	0.63	2:1	x	–

Table S4: Summary of ^{Et}**tetra·Cl$_4$** and **TBA$_2$·TP** crystallisation conditions and outcomes.

Solvent	Conc. of ^{Et}tetra·Cl$_4$ (mM)	Conc. of TBA$_2$·TP (mM)	Molar ratio	Precipitate?	Product
H_2O	10	20	1:2	x	–
	5.0	10	1:2	x	–
	2.5	5.0	1:2	x	–
	1.3	2.5	1:2	x	–
	0.63	1.3	1:2	x	–
EtOH	10	20	1:2	x	–
	5.0	10	1:2	x	–
	2.5	5.0	1:2	x	–
	1.3	2.5	1:2	x	–
	0.63	1.3	1:2	x	–
DMSO	10	20	1:2	?	amorphous solid
	5.0	10	1:2	?	amorphous solid
	2.5	5.0	1:2	?	amorphous solid
	1.3	2.5	1:2	?	amorphous solid
	0.63	1.3	1:2	?	amorphous solid

Table S5: Summary of ^{Et}**tetra·Cl$_4$** and **TBA$_2$·BPDC** crystallisation conditions and outcomes.

Solvent	Conc. of ^{Et}tetra·Cl$_4$ (mM)	Conc. of TBA$_2$·BPDC (mM)	Molar ratio	Precipitate?	Product
H_2O	10	20	1:2	x	–
	5.0	10	1:2	x	–
	2.5	5.0	1:2	x	–
	1.3	2.5	1:2	x	–
	0.63	1.3	1:2	x	–
EtOH	10	20	1:2	✓	^{Et}**tetra·(^{H}BPDC)$_4$**[a]
	5.0	10	1:2	✓	^{Et}**tetra·(^{H}BPDC)$_4$**[a]
	2.5	5.0	1:2	?	amorphous solid
	1.3	2.5	1:2	?	amorphous solid
	0.63	1.3	1:2	x	–
	0.31	0.63	1:2	x	–
DMSO	10	20	1:2	?	amorphous solid
	5.0	10	1:2	?	amorphous solid
	2.5	5.0	1:2	?	amorphous solid
	1.3	2.5	1:2	?	amorphous solid
	0.63	1.3	1:2	?	amorphous solid

[a]On one occasion we obtained this product on a small scale. Subsequent attempts to repeat this synthesis on a larger scale, using a 1:4 ratio of ^{Et}**tetra·Cl$_4$**:**TBA$_2$·BPDC**, or adding small amounts of acetic acid to partially protonate **BPDC^{2-}** were unsuccessful. These usually gave amorphous material, except when a stoichiometric amount of acetic acid was used, in which case we isolated biphenyl dicarboxylic acid.

Table S6: Summary of ^{Et}**tetra·Cl$_4$** and **TBA$_4$·TC** crystallisation conditions and outcomes.

Solvent	Conc. of ^{Et}tetra·Cl$_4$ (mM)	Conc. of TBA$_4$·TC (mM)	Molar ratio	Precipitate?	Product
H_2O	10	10	1:1	x	–
	5.0	5.0	1:1	x	–
	2.5	2.5	1:1	x	–
	1.3	1.3	1:1	x	–
	0.63	0.63	1:1	x	–
EtOH	10	10	1:1	✓	^{Et}**tetra·TC**
	5.0	5.0	1:1	✓	^{Et}**tetra·TC**
	2.5	2.5	1:1	✓	^{Et}**tetra·TC**
	1.3	1.3	1:1	✓	^{Et}**tetra·TC**
	0.63	0.63	1:1	✓	^{Et}**tetra·TC**
DMSO	10	10	1:1	?	amorphous solid
	5.0	5.0	1:1	?	amorphous solid
	2.5	2.5	1:1	?	amorphous solid
	1.3	1.3	1:1	?	amorphous solid
	0.63	0.63	1:1	?	amorphous solid

1.4 Characterisation data for hydrogen bonded networks

1.4.1 Characterisation data for ^{Et}biphen·TP

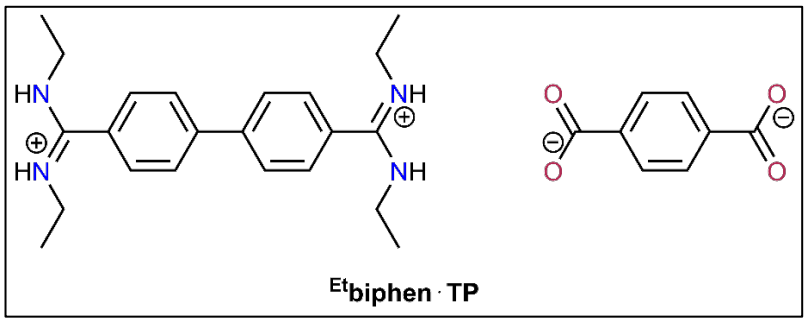

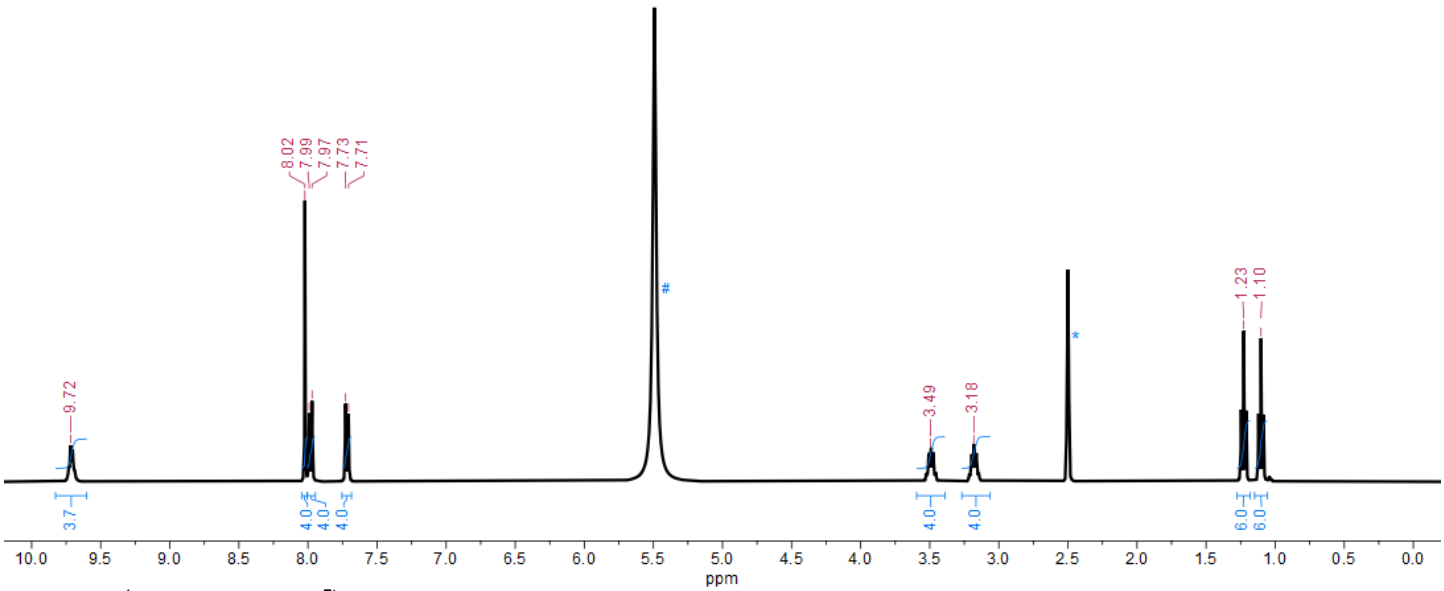

Figure S19. ^{1}H NMR spectrum of ^{Et}**biphen·TP**, * indicates residual NMR solvent peak, # indicates water (d_6-DMSO containing a drop of $DCl_{(aq)}$, 400 MHz, 298 K). Note that in the solid state this compound has the *E/E* conformation, but in the ^{1}H NMR spectrum shown above it has the *E/Z* conformation, as indicated by two sets of peaks for the ethyl hydrogen atoms.

As shown in Figure S20, ^{Et}**biphen·TP** rearranges to an unknown crystalline phase upon drying.

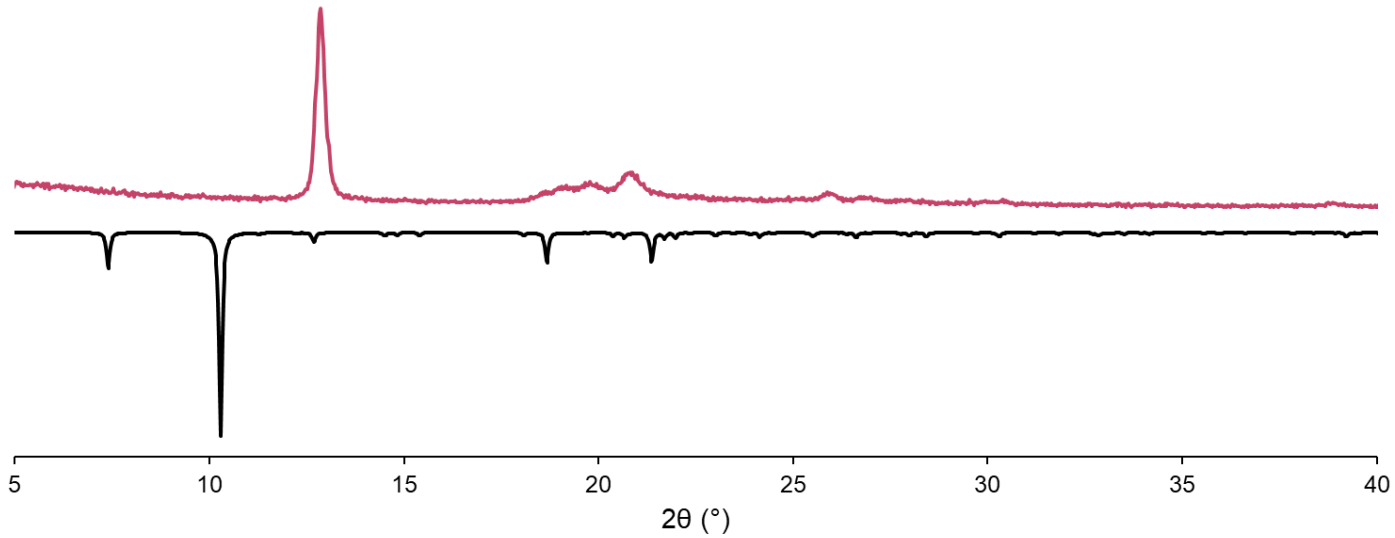

Figure S20. PXRD trace of ^{Et}**biphen·TP** (up, maroon) and that calculated based on SCXRD data (down, black).

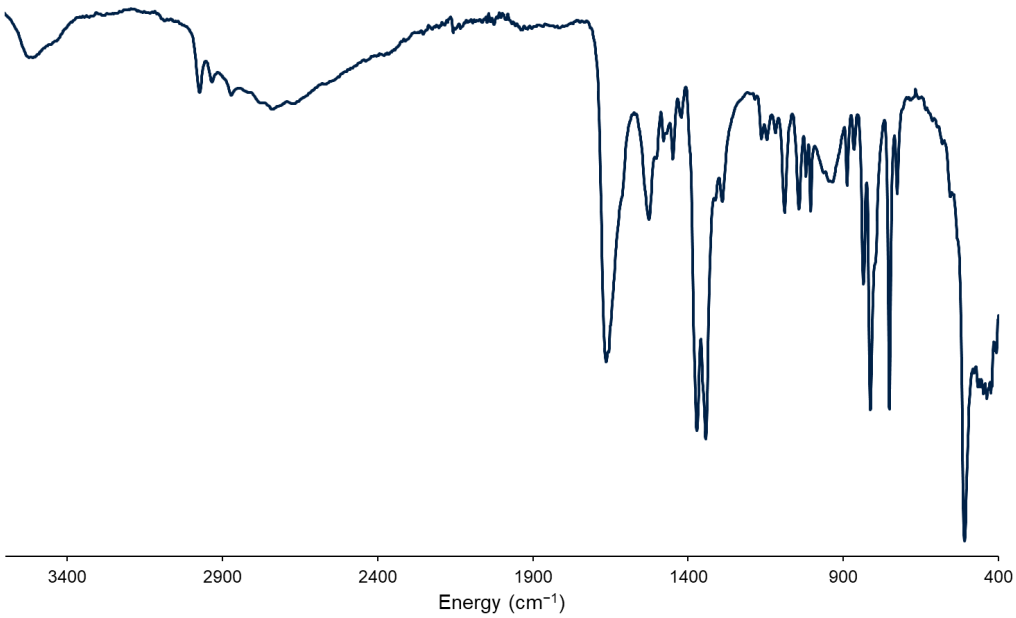

Figure S21. IR spectrum of ^{Et}**biphen·TP**.

1.4.2 Characterisation data for ^{Et}tetra·TC

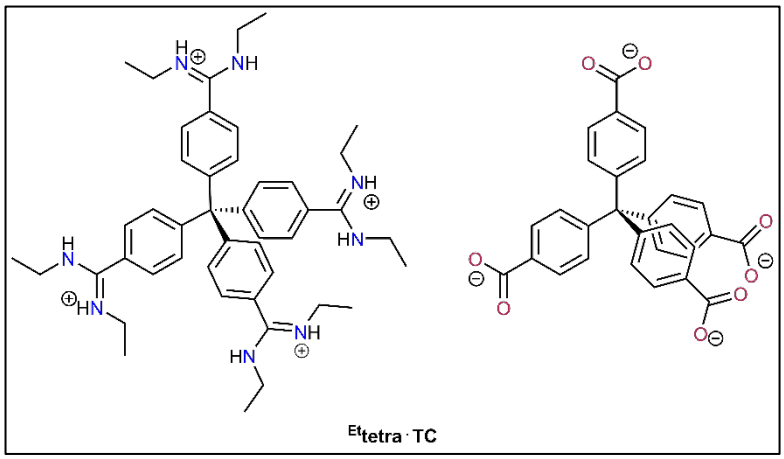

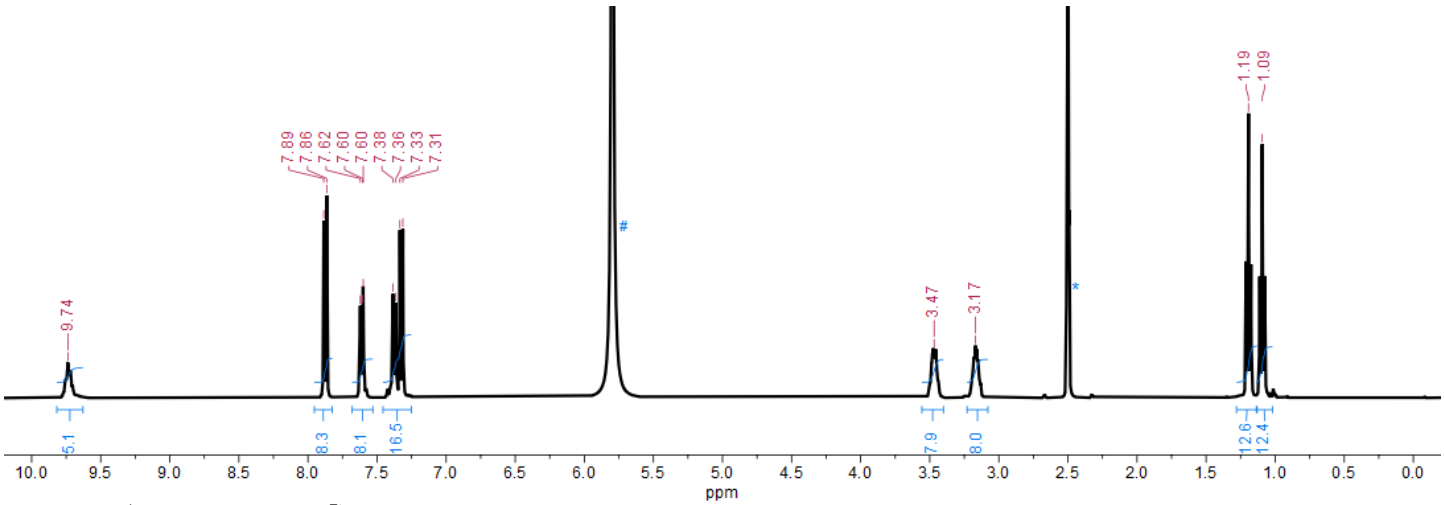

Figure S22. ^{1}H NMR spectrum of ^{Et}**tetra·TC**, * indicates residual NMR solvent peak, # indicates water (d_6-DMSO containing a drop of $DCl_{(aq)}$, 400 MHz, 298 K).

PXRD of air-dried **^{Et}tetra·TC** showed a weak peak at 2θ ~ 7°, but grinding the sample caused this peak to disappear (Figure S23). We attribute this peak to small areas within the crystals containing trapped solvent and thus retaining some crystallinity, with grinding resulting in release of this trapped solvent and a complete loss of crystallinity. ^{1}H NMR spectroscopy of the acid-digested framework (Figure S22) indicates only a trace of ethanol is present so presumably these crystalline domains containing trapped ethanol represent a very small amount of the total structure. This is consistent with the low intensity of the observed peak.

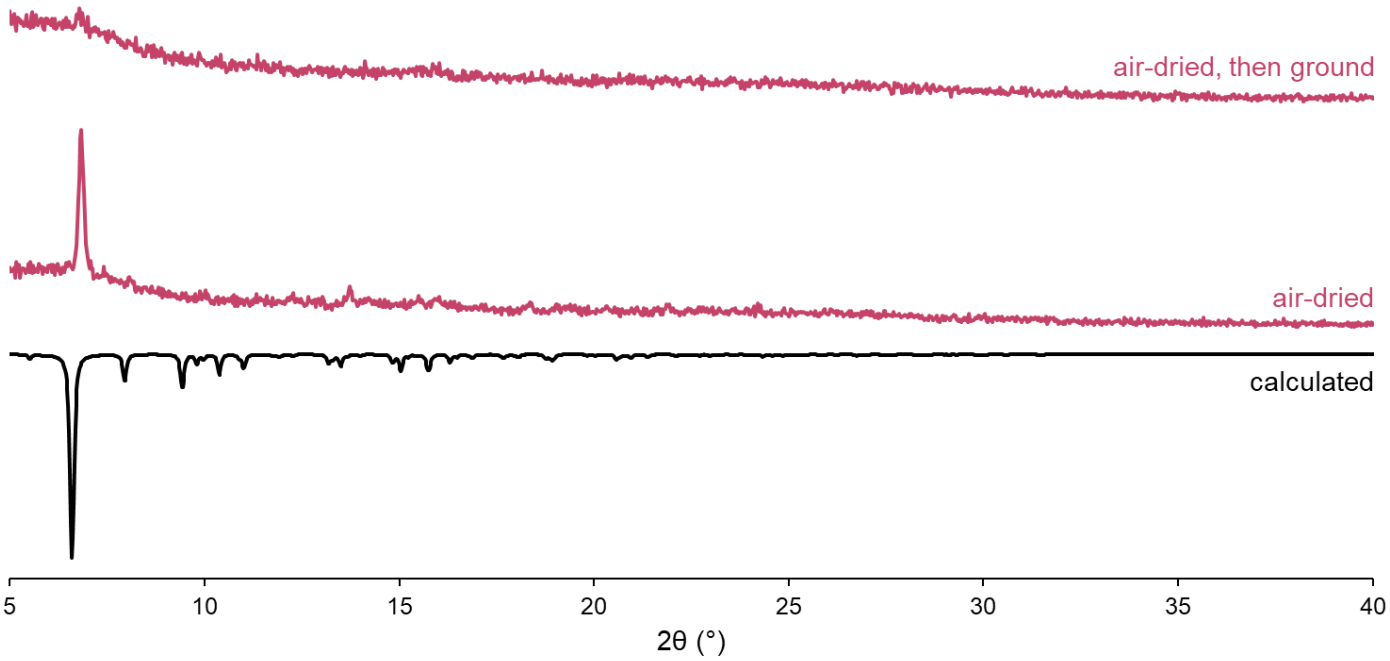

Figure S23. PXRD trace of **^{Et}tetra·TC** (up, maroon) and that calculated based on SCXRD data (down, black).

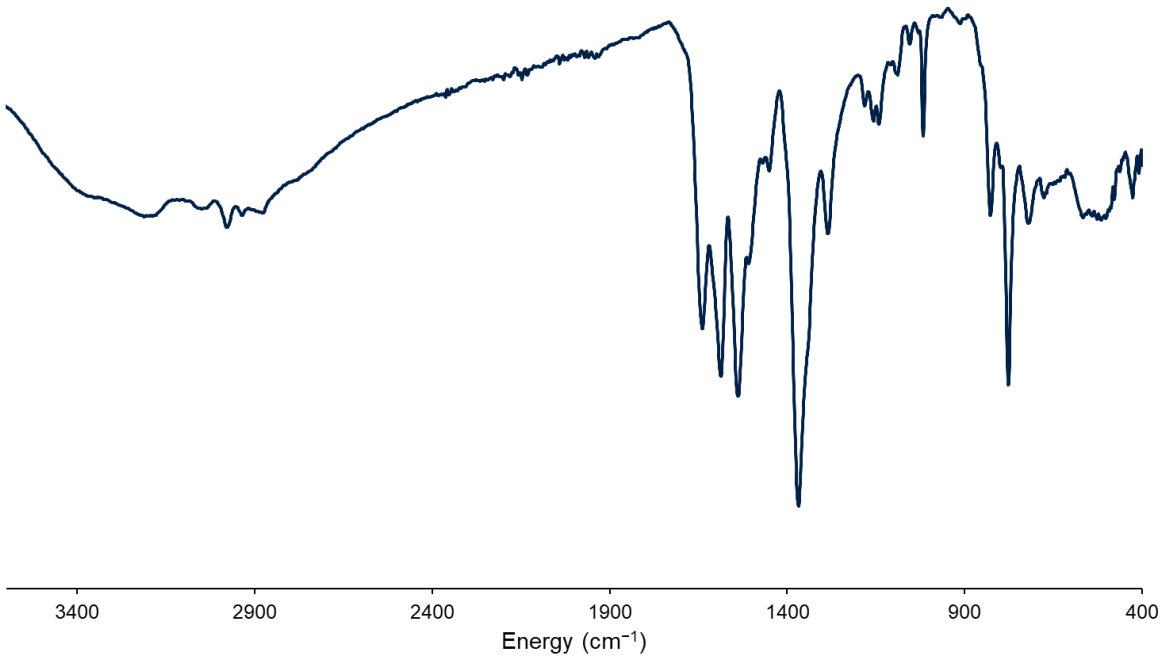

Figure S24. IR spectrum of **^{Et}tetra·TC**.

2 Solution NMR studies

2.1 General remarks

Solution studies were conducted to investigate the energy barrier to change between *E/Z* and *E/E* conformations of the diethylamidinium group, and to study the effect of carboxylate binding to the diethylamidinium groups. We did this using benzoate as a model carboxylate (using commercially available **Na·BzO** for studies in D_2O and commercially available **TBA·BzO** for studies in organic solvents). Where possible we used the simple model compound, **^{Et}model·BPh_4**; however this compound is not soluble in water (and we were unable to prepare a water-soluble salt of it), so for studies in water we used **^{Et}biphen·Cl_2**.

2.2 Solution studies in D_2O

2.2.1 Variable temperature ^{1}H NMR spectra of ^{Et}biphen·Cl_2 in D_2O

The ^{1}H NMR spectrum of a 2.0 mM solution of **^{Et}biphen·Cl_2** in D_2O was recorded at various temperatures (Figure S25). The spectra were referenced to the residual NMR solvent signal, which was approximately corrected for temperature changes, as described by Gottlieb, Nudelman and co-workers.[1] As can be seen, no coalescence of the peaks is observed, suggesting that the E/Z conformation remains even at high temperatures. At the highest temperature studied (353 K), there is evidence of very slight broadening of the ethyl peaks, suggesting that exchange is starting to approach the NMR timescale.

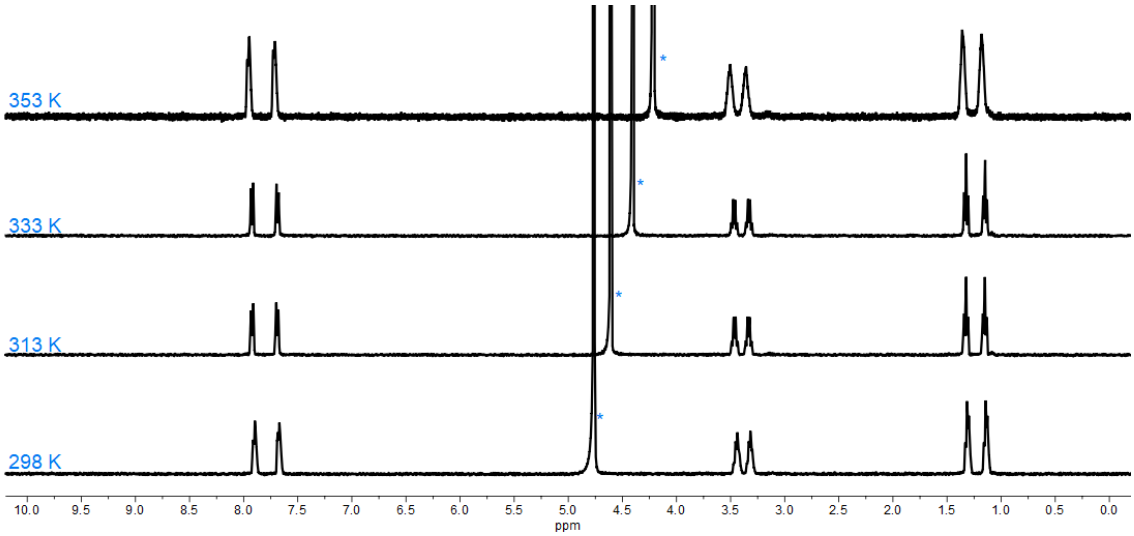

Figure S25. ^{1}H NMR spectra of **^{Et}biphen·Cl_2** at various temperatures in D_2O, * indicates residual NMR solvent signal (400 MHz, 298 K, 2.0 mM in D_2O).

2.2.2 Interaction of ^{Et}biphen·Cl_2 with benzoate in D_2O

As shown in Figure S26, addition of BzO^- in D_2O did not have any effect on the E/Z conformation of **^{Et}biphen·Cl_2** even at very high excess of benzoate. We attribute peak shifts at 100 equivalents of benzoate to the change in pH of the solution.

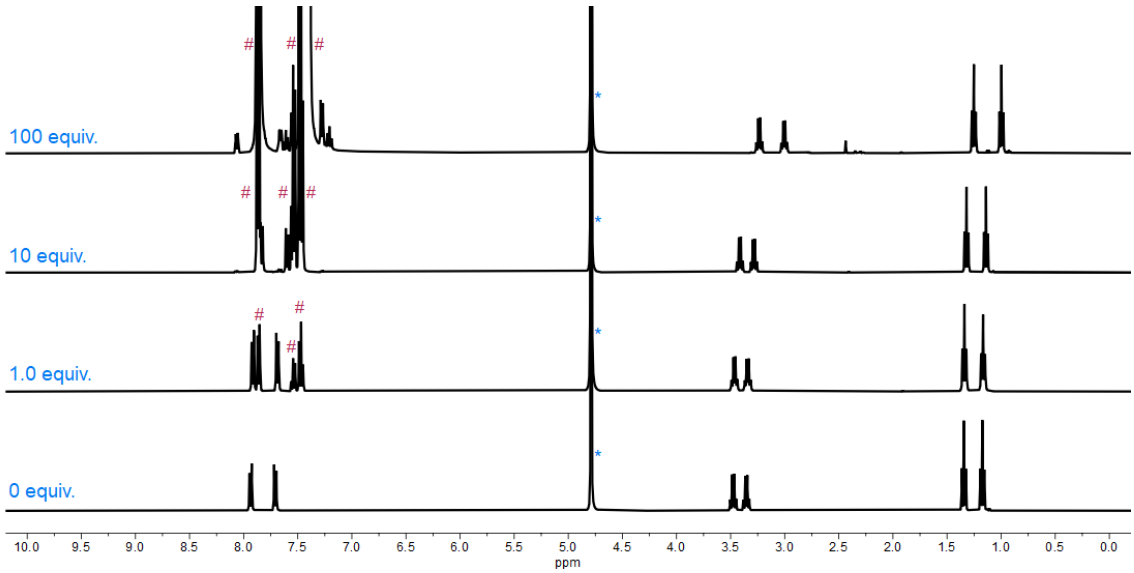

Figure S26. ^{1}H NMR spectra of **^{Et}biphen·Cl_2** in the presence of 0, 10 and 100 equivalents of sodium benzoate, * indicates residual NMR solvent peak, # indicates peaks due to benzoate anion (400 MHz, 298 K, 2.0 mM **^{Et}biphen·Cl_2** in D_2O).

2.3 Solution studies in d_6-DMSO

Addition of aliquots of a 100 mM solution **TBA·BzO** to a 2.0 mM solution of ^{Et}**model·BPh$_4$** in d_6-DMSO resulted in the peak shifts shown in Figures S27 and S28. The movement of the two aromatic C–H resonances was fitted to a 1:1 binding model in *Bindfit* (Figure S29).[3] This gave an association constant of 739 ± 77 M^{-1}. Full binding and fitting data are available at http://app.supramolecular.org/bindfit/view/81be6c8e-9663-415e-b391-0f4d598b97bd.

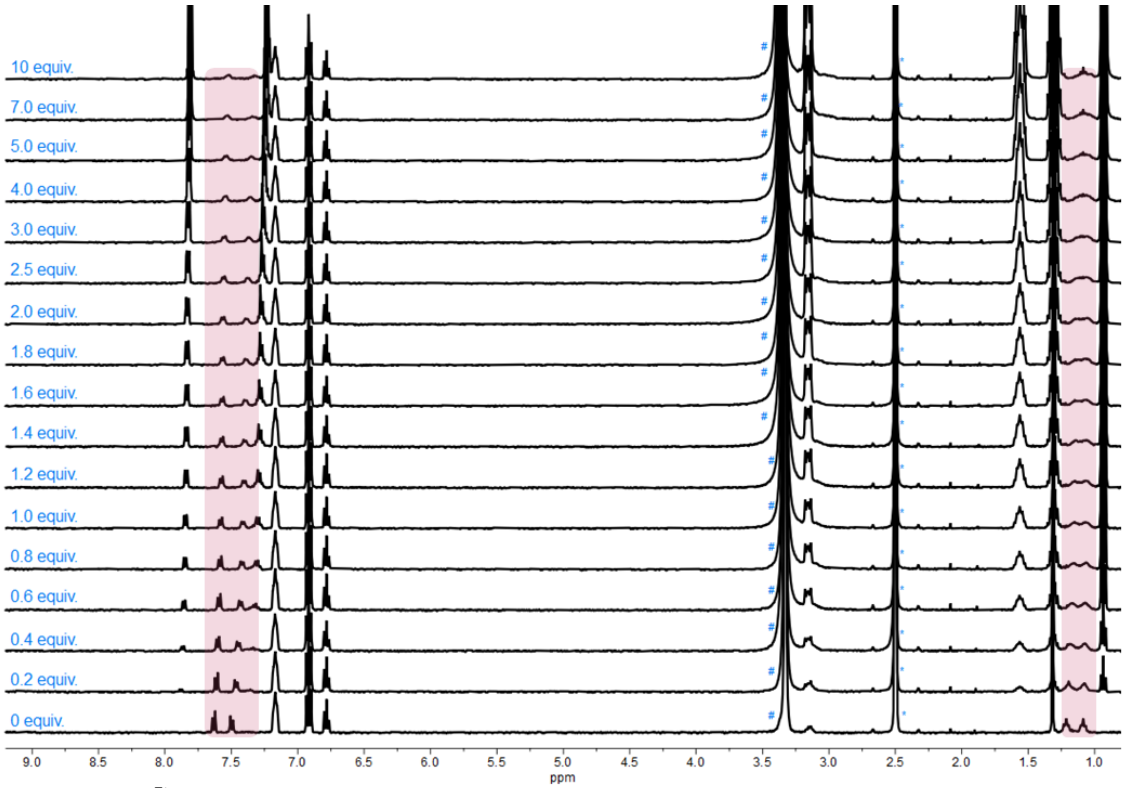

Figure S27. ^{1}H NMR spectra of ^{Et}**model·BPh$_4$** in the presence of varying numbers of equivalents of **TBA·BzO**, * indicates residual NMR solvent peak, # indicates water. Peaks corresponding to ^{Et}**model$^+$** are highlighted (the ethyl CH_2 signals are not highlighted as these coincide with the TBA cation's N^+–CH_2 peak, other peaks correspond to TBA^+ cation and BPh_4^- and BzO^- anions (400 MHz, 298 K, d_6-DMSO).

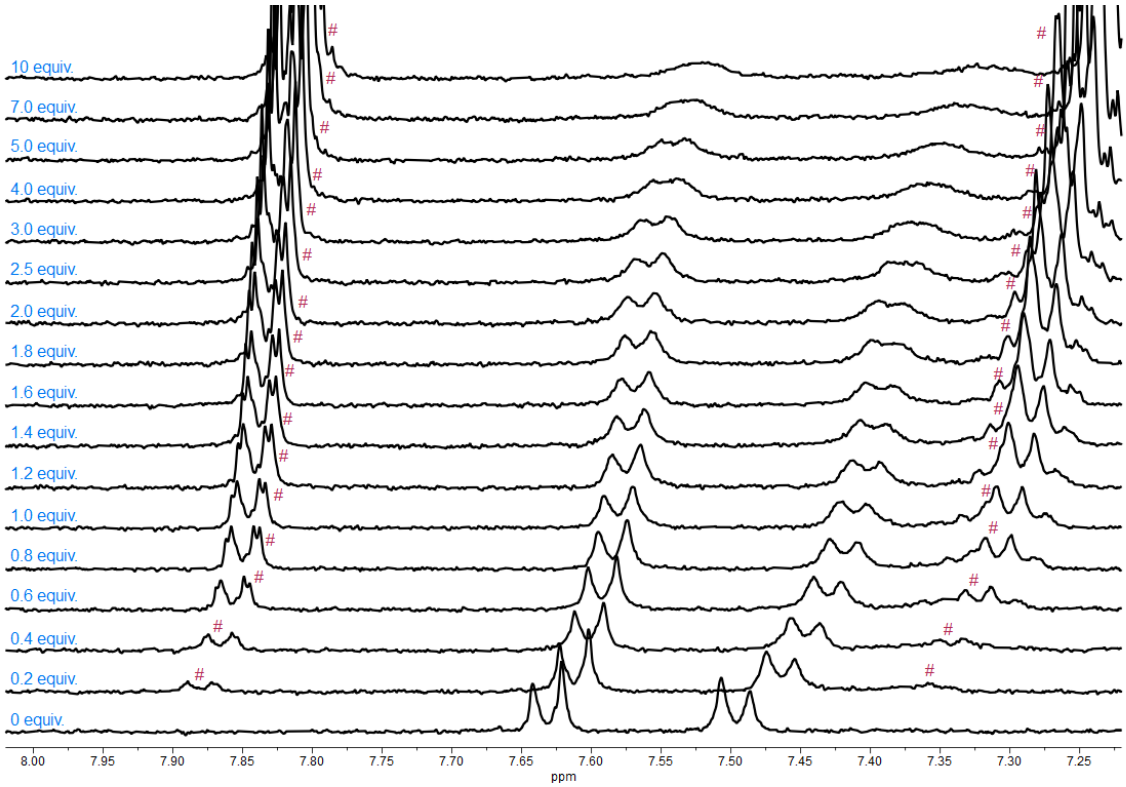

Figure S28. Partial ^{1}H NMR spectra of ^{Et}**model·BPh$_4$** in the presence of varying numbers of equivalents of **TBA·BzO**. Peaks corresponding to BzO^- anions are indicated with # symbols (400 MHz, 298 K, d_6-DMSO).

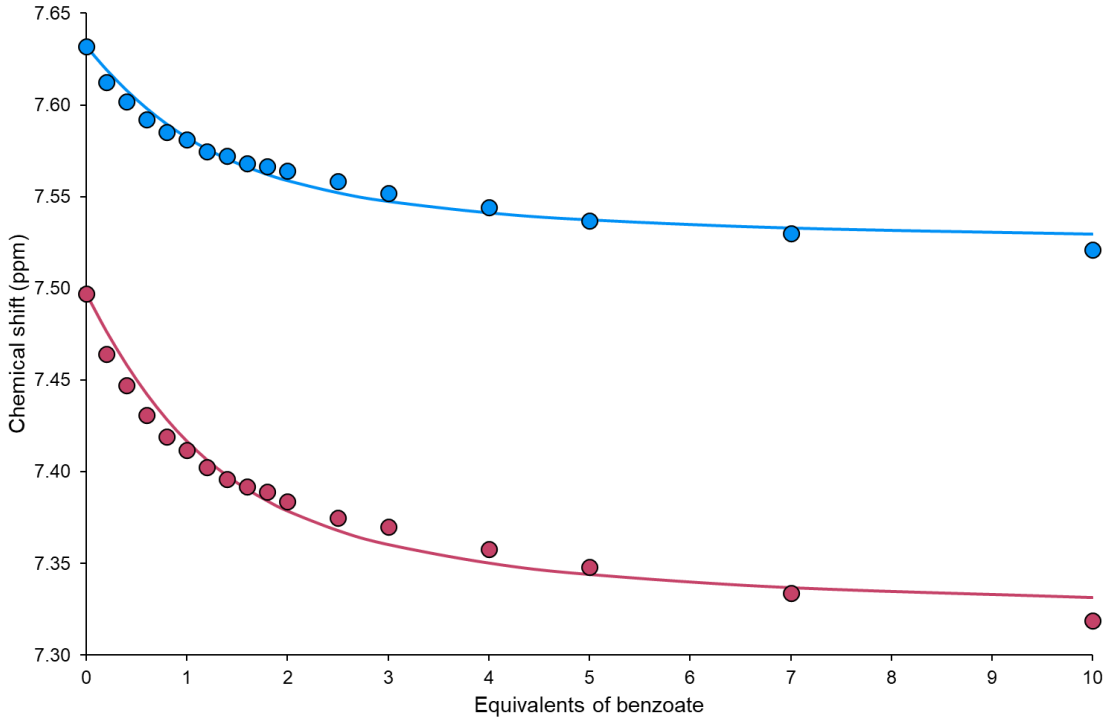

Figure S29. Movement of aromatic C–H resonances of ^{Et}**model·BPh$_4$** upon addition of **TBA·BzO** in d_6-DMSO. Circles represent data, lines represent 1:1 binding isotherm fitted in *Bindfit*.[3]

2.4 Solution studies in CD_3CN

2.4.1 Interaction of ^{Et}model·BPh_4 with benzoate in CD_3CN at 298 K

Addition of aliquots of a 100 mM solution **TBA·BzO** to a 2.0 mM solution of ^{Et}**model·BPh$_4$** in CD_3CN resulted in the peak shifts shown in Figure S30. The aromatic C–H signals broaden, as do the ethyl groups. Because of this it was not possible to determine a quantitative association constant. Qualitatively, binding appears to be strong, as indicated by the complete disappearance of the ethyl CH_2 signals at ~ 3.3 ppm and appearance of a new signal at 2.9 ppm after one equivalent of anion (although this overlaps with the TBA cation's N^+–CH_2 signal). Further information about binding strength was determined from low temperature ^{1}H NMR spectroscopy (Section 2.4.2).

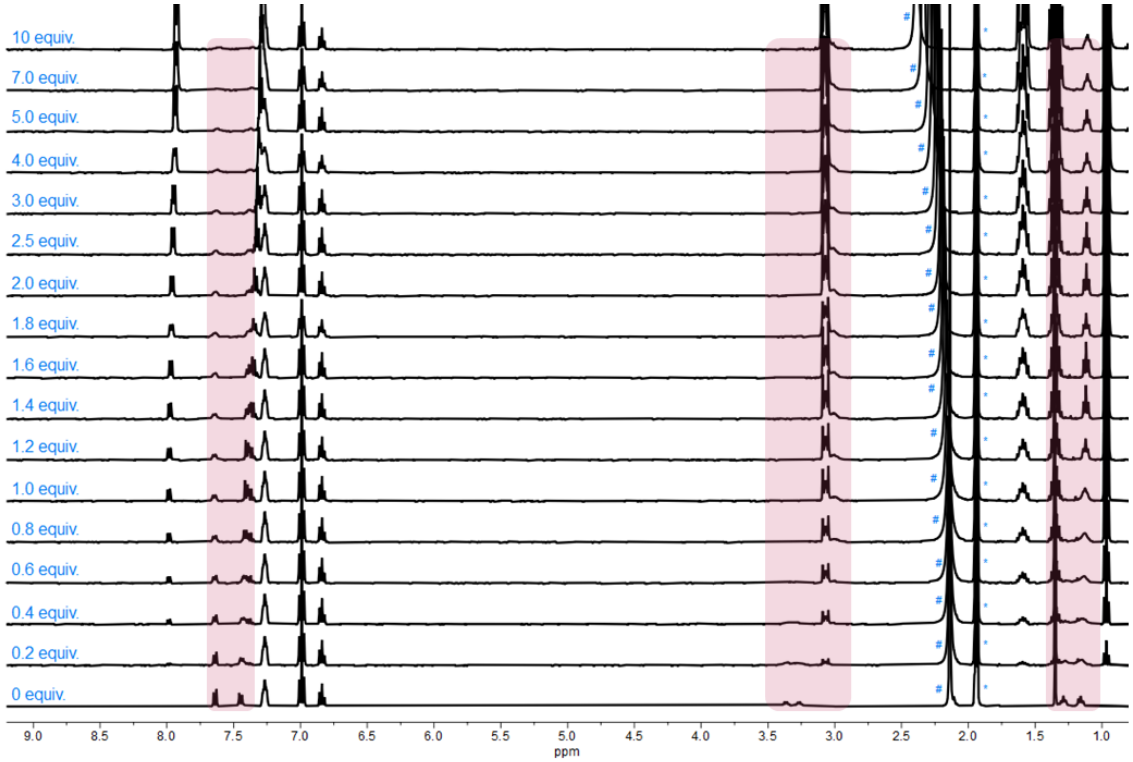

Figure S30. ^{1}H NMR spectra of ^{Et}**model·BPh$_4$** in the presence of varying numbers of equivalents of **TBA·BzO**, * indicates residual NMR solvent peak, # indicates water. Peaks corresponding to ^{Et}**model$^+$** are highlighted, other peaks correspond to TBA^+ cation and BPh_4^- and BzO^- anions (400 MHz, 298 K, CD_3CN).

2.4.2 Low temperature study of interaction of ^{Et}model·BPh_4 with benzoate in CD_3CN

The ^{1}H NMR spectrum of **^{Et}model·BPh_4** and one equivalent of **TBA·BzO** was recorded at room temperature, and at lowered temperatures (Figure S31). As was previously observed with **^{Me}model·BPh_4**,[2] at low temperatures peaks in slow exchange are observed, which we attribute to complexed and free **^{Et}model$^+$**. The complexed **^{Et}model$^+$** is in the E/E conformation, while free **^{Et}model$^+$** adopts the E/Z conformation (interestingly this was not observed with **^{Me}model$^+$** where the free complex appeared to still have the E/E conformation).[2]

The presence of **^{Et}model·BzO** and "free" **^{Et}model$^+$** in slow exchange at low temperatures (Figure S31) allows estimation of the association constant of integration of the two sets of signals. Integrating the CH_2 resonances (as these are well-isolated in the spectrum) gives ratios of complexed to uncomplexed **^{Et}model$^+$** of 7.0:1 at 253 K and 7.4:1 at 233 K. Knowing the total concentration of **^{Et}model$^+$** (1.96 mM), allows calculation of complexed and uncomplexed **^{Et}model$^+$** (0.245 and 1.715 mM, respectively at 253 K; 0.233 and 1.727 mM, respectively at 233 K). This allows estimation of K_a as 28,600 M^{-1} at 253 K and 31,800 M^{-1} at 233 K. Given the limited accuracy of integrating ^{1}H NMR spectra, we stress that these are estimates only, however they are consistent with strong binding, as would be expected for a charged host in CD_3CN. These values are also similar to those calculated for **^{Me}model·BPh_4** under the same conditions (K_a = 35,000 M^{-1} at 253 K and 37,600 M^{-1} at 233 K).[2]

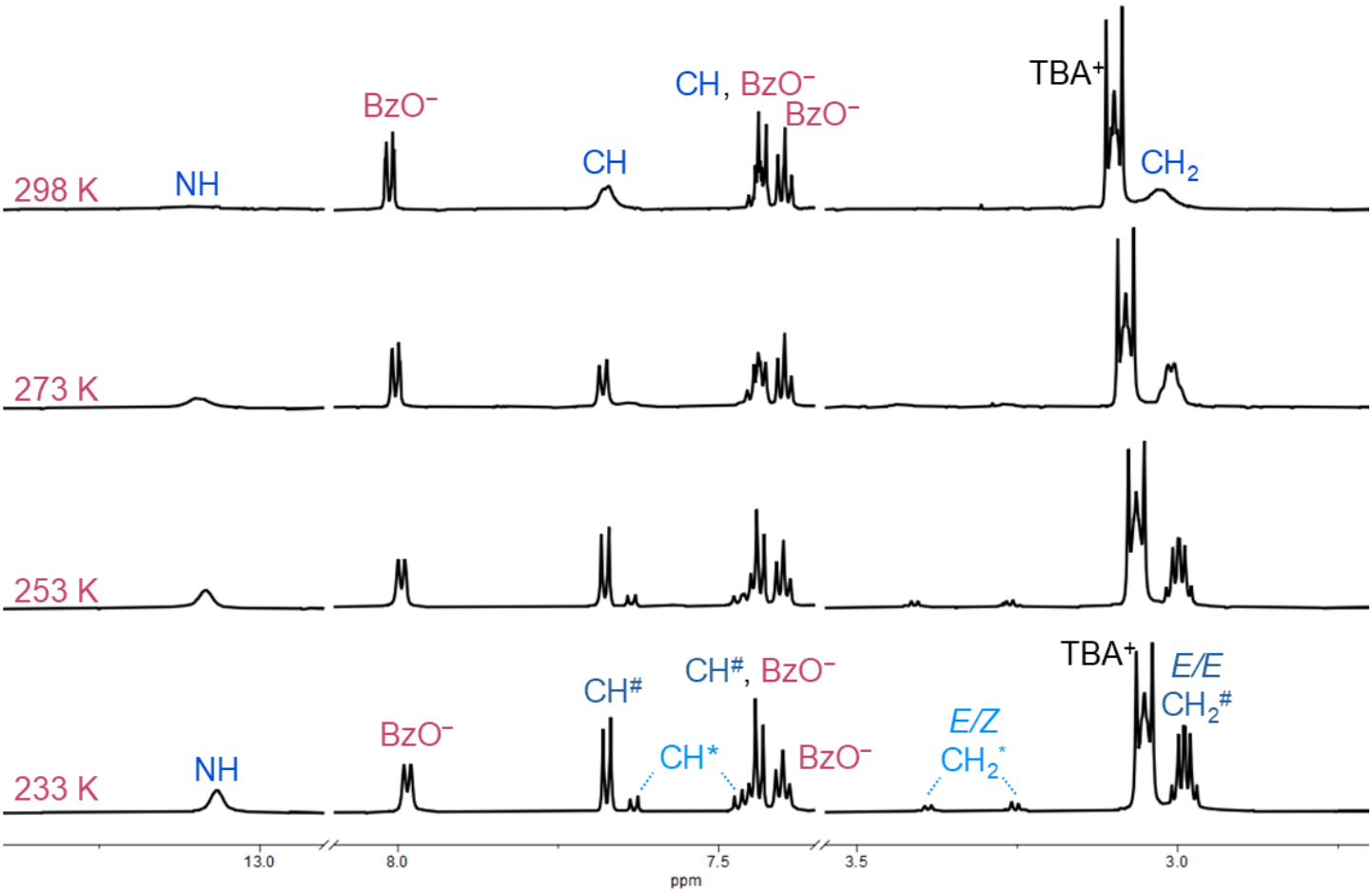

Figure S31. ^{1}H NMR spectra of a 2.0 mM solution of **^{Et}model·BPh_4** and 1.0 equivalents of **TBA·BzO** at various temperatures (700 MHz, CD_3CN). Peaks in the low temperature spectrum assigned to complexed **^{Et}model·BzO** are labelled # and peaks assigned to free **^{Et}model$^+$** are labelled *.

3 Single crystal X-ray diffraction studies

3.1 General remarks

Diffraction data for all were collected on an Oxford Diffraction SuperNova instrument using Cu or Mo radiation at 150 K. Raw frame data (including data reduction, interframe scaling, unit cell refinement and absorption corrections) were processed using CrysAlis Pro.[4] All structures were solved using Superflip[5] or ShelXT[6] and refined against F^2 within the CRYSTALS suite.[7] Further details about individual structures are given in Sections 3.2 – 3.6.

Full crystallographic data in CIF format are provided as Supporting Information (CCDC Numbers: 2503994 – 2503998) and selected crystallographic data are provided in Table S7.

Table S7. Selected crystallographic data.

Compound	**^{Et}biphen·Cl$_2$**	**^{Et}biphen·TP** [a]	**^{Et}biphen·BPDC**	**^{Et}tetra·(^{H}BPDC)$_4$**	**^{Et}tetra·TC** [a]
Radiation	Cu (λ = 1.54184 Å)	Mo (λ = 0.71073 Å)	Mo (λ = 0.71073 Å)	Cu (λ = 1.54184 Å)	Cu (λ = 1.54184 Å)
a (Å)	7.38710(10)	9.4959(13)	10.9536(9)	22.70732(9)	30.0803(5)
b (Å)	17.4215(2)	17.181(2)	12.2674(12)	22.70732(9)	26.6383(5)
c (Å)	18.6866(3)	23.879(2)	12.3465(8)	17.56650(11)	26.8475(5)
α (°)	90	90	92.853(6)	90	90
β (°)	100.1555(14)	90	98.138(6)	90	90
γ (°)	90	90	105.889(8)	90	90
Unit cell volume (Å^3)	2367.18(6)	3895.8(8)	1572.7(2)	9057.68(9)	21512.6(7)
Crystal system	monoclinic	orthorhombic	triclinic	tetragonal	orthorhombic
Space group	*P2$_1$/c*	*Pnna*	*P–1*	*I4$_1$/a*	*Pbcn*
Formula	$C_{22}H_{32}N_4{\cdot}2Cl{\cdot}H_2O$	$C_{22}H_{32}N_4{\cdot}C_8H_4O_4$ ·*solvents*[a]	$C_{22}H_{34}N_4{\cdot}C_{14}H_8O_4$	$C_{45}H_{64}N_8{\cdot}(C_{14}H_9O_4)_4$	$C_{45}H_{64}N_8{\cdot}C_{29}H_{16}O_8{\cdot}$ *solvents*[a]
Formula weight	441.44	516.64	592.74	1681.96	1209.50
Z	4	4	2	4	8
Reflections (all)	26689	19786	13617	67557	88872
Reflections (unique)	4286	3580	3818	4625	13143
R_{int}	0.055	0.150	0.127	0.038	0.056
R_1 [$I > 2\sigma(I)$]	0.038	0.185	0.068	0.042	0.162
wR_2 (all data)	0.095	0.234	0.149	0.129	0.216
CCDC number	2503994	2503995	2503996	2503997	2503998

[a] PLATON-SQUEEZE[8] was used.

3.2 Structure of ^{Et}biphen·Cl$_2$

Crystals were grown by adding THF to a solution of the compound in methanol/water. Crystals diffracted well and refinement proceeded smoothly. N–H and O–H hydrogen atoms were visible in the difference map and their positions were refined with restraints.[9] C–H positions were initially refined with restraints and then these positions were used as the basis for a riding model.[9] Otherwise, it was not necessary to use any crystallographic restraints in the refinement.

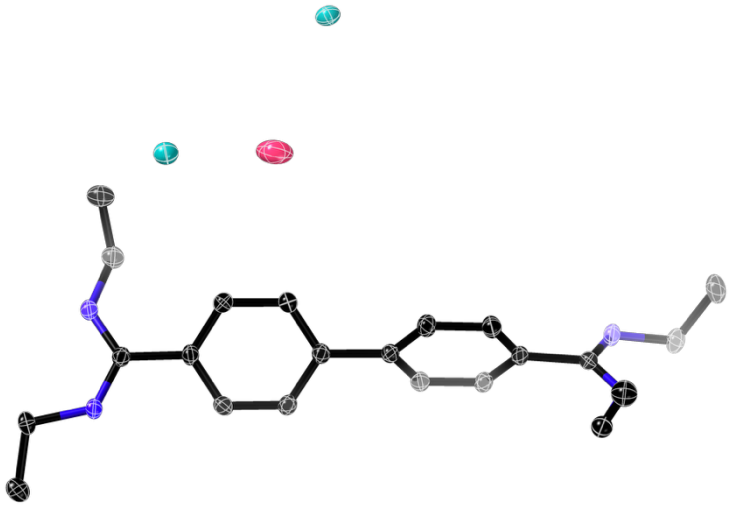

Figure S32. Thermal ellipsoid plot showing the asymmetric unit of **^{Et}biphen·Cl$_2$**; ellipsoids are shown at 50% probability, hydrogen atoms are omitted.

3.3 Structure of ^{Et}biphen·TP

Crystals were grown by mixing solutions of **^{Et}biphen·Cl$_2$** and **TBA$_2$·TP** in ethanol (final concentration = 10 mM in each component). Crystals diffracted relatively weakly and even with long exposure times, some reflections were quite weak. The space group was quite ambiguous and it was initially difficult to solve the structure. Overall, the data are of limited quality, so while the overall molecular structure and packing can be determined unambiguously, detailed inferences should not be drawn about bond lengths or hydrogen bonding parameters.

The structure contains diffuse electron density, which appears to arise from disordered solvent molecules. This could not be resolved and so PLATON-SQUEEZE[8] was used to include this electron density in the refinement.

The ethyl groups of the diethylamidinium moieties are disordered. This was modelled by having two positions for each terminal CH_3 group (relative occupancies: 0.75:0.25 for one group and 0.5:0.5 for the other), with restraints applied to the bond lengths and angles of the diethylamidinium groups. Thermal and vibrational ellipsoid restraints were used on all atoms of the diamidinium molecule, with CRYSTALS QISO restraints (similar to SHELX ISOR restraints) used on the atoms of the disordered ethyl groups. The terephthalate anion was better-behaved, but it was necessary to use restraints on the C–C bonds between the phenyl rings and the carboxylate groups. C–H and N–H hydrogen atoms were inserted at calculated positions (N–H distances = 0.86 Å, C–H distances = 0.95 Å), and these positions used as the basis for a riding model.[9]

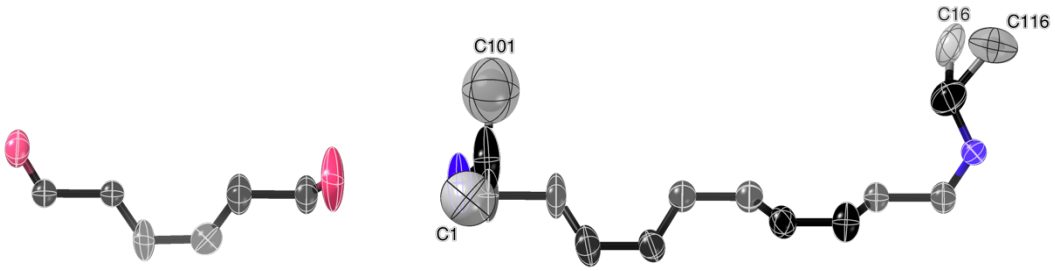

Figure S33. Thermal ellipsoid plot showing the asymmetric unit of **^{Et}biphen·TP**; ellipsoids are shown at 50% probability, hydrogen atoms are omitted. Two different positions of disorder are shown in grey, with the disordered atoms labelled.

3.4 Structure of ^{Et}biphen·BPDC

Crystals were grown by mixing solutions of **^{Et}biphen·Cl$_2$** and **TBA$_2$·BPDC** in ethanol (final concentration = 10 mM in each component). Crystals diffracted relatively weakly and even with long exposure times, some reflections were quite weak. N–H hydrogen atoms were inserted at calculated positions and then their positions were refined with restraints on N–H distances and C–N–H angles.[9] C–H positions were initially refined with restraints and then these positions were used as the basis for a riding model.[9] Otherwise, it was not necessary to use any crystallographic restraints in the refinement.

CheckCIF highlights possible additional symmetry, however this does not appear to be genuine. There is a small amount of residual electron density, but this appears to be noise rather than missed solvent or disorder.

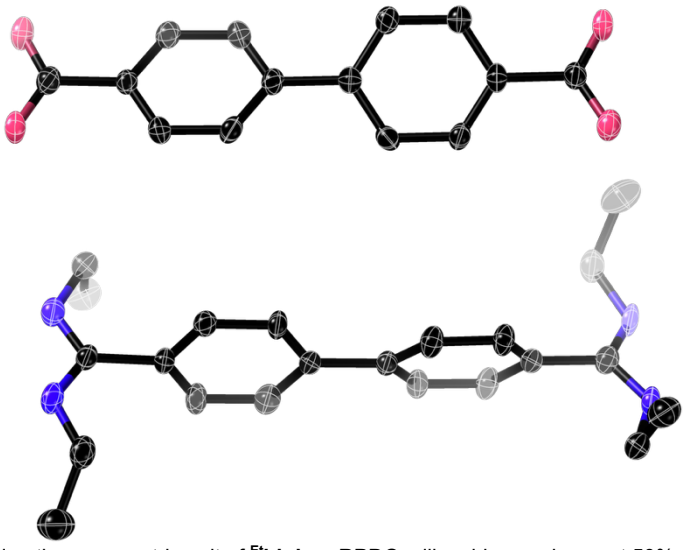

Figure S34. Thermal ellipsoid plot showing the asymmetric unit of **^{Et}biphen·BPDC**; ellipsoids are shown at 50% probability, hydrogen atoms are omitted.

3.5 Structure of ^{Et}tetra·(^{H}BPDC)$_4$

Crystals were grown by mixing one equivalent of **^{Et}tetra·Cl$_4$** and two equivalents of **TBA$_2$·BPDC** in ethanol (final concentration = 5.0 mM in **^{Et}tetra·Cl$_4$**). The asymmetric unit contains one quarter of a molecule of **^{Et}tetra^{4+}** and one dicarboxylate molecule, which has been spontaneously mono-protonated, *i.e.* **^{H}BPDC^{-}**. The structure contains very small voids, however these appear to be empty (PLATON-SQUEEZE[8] analysis indicates 16 voids in the P1 unit cell, each with volumes 28 – 32 Å^3 and each containing 1 electron).

One of the ethyl groups is disordered. This was modelled over two positions (occupancies = 0.5:0.5). It was necessary to add restraints to the C–N and C–C bond lengths, and N–C–C angles of the disordered ethyl groups to achieve a sensible refinement.

Amidinium N–H groups and the carboxylic acid O–H hydrogen atom were clearly visible in the difference map and their positions were refined with restraints.[9] C–H positions were initially refined with restraints and then these positions were used as the basis for a riding model.[9]

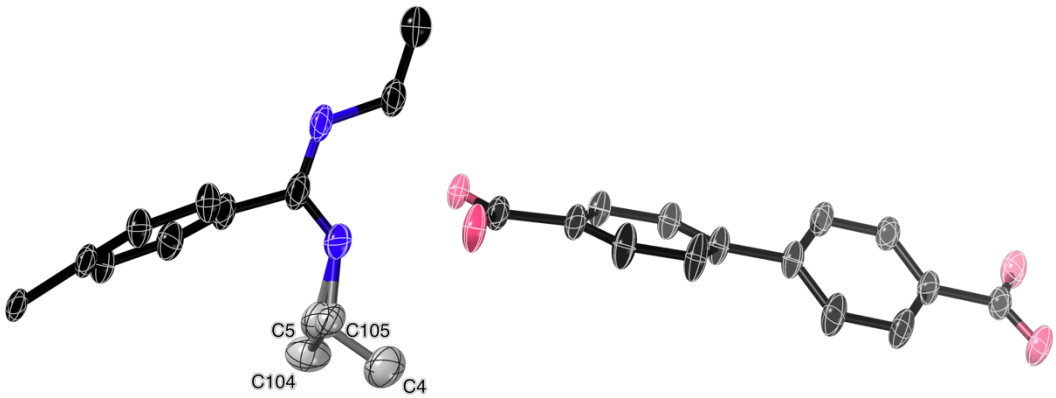

Figure S35. Thermal ellipsoid plot showing the asymmetric unit of **^{Et}tetra·(^{H}BPDC)$_4$**; ellipsoids are shown at 50% probability, hydrogen atoms are omitted. Two different positions of disorder are shown in grey, with the disordered atoms labelled.

3.6 Structure of ^{Et}tetra·TC

Crystals were grown by mixing equimolar solutions of **^{Et}tetra·Cl$_4$** and **TBA$_4$·TC** in ethanol (final concentration = 10 mM in each component). Crystals were large but appeared to lose solvent very rapidly. Even working as quickly as possible to minimise solvent loss, diffraction was of limited quality and no diffraction could be obtained beyond 0.95 Å. We collected several datasets for these crystals at beamline MX2[10] of the Australian Synchrotron, but even using synchrotron radiation we were not able to obtain diffraction data at higher resolution. The best quality data was obtained using home-source radiation, and so this was used in the final refinement. The low diffraction resolution and the presence of relatively large voids filled with diffuse electron density mean the structure is of relatively low quality. Nevertheless, the molecular structure and packing can be determined unambiguously.

The diffuse electron density was included in the model using PLATON-SQUEEZE.[8] It was necessary to add restraints to all C–C and C–N bond lengths as well as some phenyl ring C–C–C angles in order to achieve a sensible refinement. Similarity restraints were added to thermal and vibrational ellipsoid parameters.

Due to the limited quality of the data, all hydrogen atoms were inserted at calculated positions and ride on the attached non-H atoms (C–H distances = 0.95 Å, N–H distances = 0.86 Å).

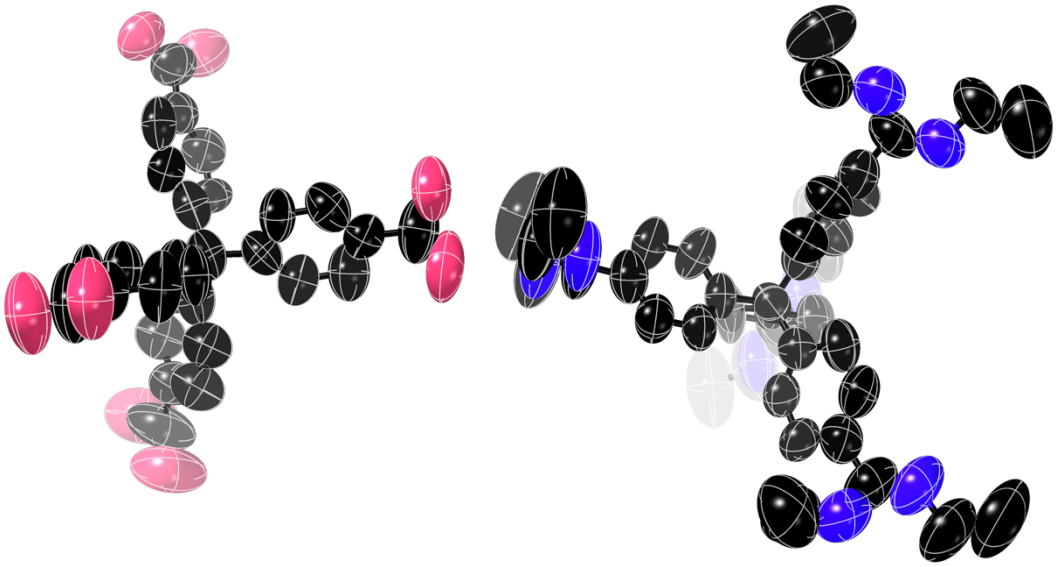

Figure S36. Thermal ellipsoid plot showing the asymmetric unit of **^{Et}tetra·TC**; ellipsoids are shown at 50% probability, hydrogen atoms are omitted.

4 Cambridge Structural Database searches

4.1 Substituent effect on conformation search parameters

The Cambridge Structural Database[11] (CSD) Version 6.00 (April 2025) was searched using the fragment shown in Figure S37. This gave a total of 38 crystal structures, which were analysed manually. This revealed that two structures actually contained either Si or P atoms directly bonded to the amidinium nitrogen atoms and so these were discarded to give a total of 36 structures. Some of these had multiple amidinium groups in the asymmetric unit, but in all cases all amidinium groups in the asymmetric unit had the same conformation as each other. Note that these search results do not include 15 X-ray crystal structures from our recent paper on dimethylamidiniums.[2]

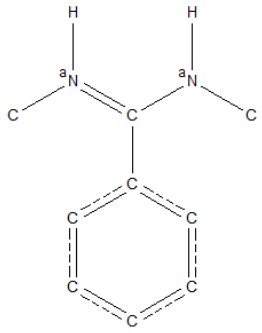

Figure S37. Search fragment used to search the CSD; superscript a indicates the atom had to be acyclic (to avoid obtaining imidazole derivatives in the search results).

4.2 Substituent effect on conformation search results

The search results are summarised in Table S8. There are clearly multiple factors at play in determining the amidinium conformation including the amidinium substituent, anion used, and the solvent used for crystallisation. While this means definitive determinants for conformation cannot be elucidated, it is clear that the *E/E* and *E/Z* conformations must be relatively similar in energy as both are frequently observed (*E/E* in 16 structures, *E/Z* in 17 structures). The *Z/Z* has not yet been observed with alkyl-substituted amidiniums but occurs relatively frequently among the small number of aryl-substituted amidiniums.

Note that 15 crystal structures from our recent paper on dimethylamidiniums are not included in this table. Four of these were chloride salts and the other 11 were polycarboxylate salts; all had the *E/Z* conformation.

Table S8. X-ray crystal structures of alkyl- and aryl-substituted amidiniums in the CSD.

CSD code[a]	Amidinium N-substituents	Anion	Conformation
AGEMOO	^{i}Pr	$EtAlCl_3^-$	E/Z
AHOQAS	^{t}Bu	$BArF^-$	E/Z
AQEVAT	Et	ferrocenecarboxylate	E/E
ARITIG	^{i}Pr	anionic manganese complex	E/E
ATOFAT	MeBn	$BINOL^-$	E/E
AXIYEN	^{n}Pr	PF_6^-, BPh_4^-	E/Z
GAQZAA	MeBn	large organic carboxylate	E/E
GIHZII	^{t}Bu	$CF_3SO_3^-$	E/Z
GIZDIE	^{i}Pr	BPh_4^-	E/E
GOJSOO	Me	$oxalate^{2-}$	E/Z
GOJSUU	Me	benzene-1,4-dicarboxylate	E/Z
GOJTEF	Me	Cl^-	E/Z
GOJTIJ	Me	BF_4^-	E/Z
IBIDUV	Et	adamantanedicarboxylate	E/E
IBIFAD	Et	octanedicarboxylate	E/E
IBIFEH	Et	nonanedicarboxylate	E/E
JAXFUN	^{t}Bu	$GaCl_4^-$	E/Z
JONVAL	^{i}Pr	$CF_3SO_3^-$	E/Z
PICLAP	MeBn	benzene-1,3,5-tricarboxylate	E/Z
PIVVOI	cyclohexyl	Cl^-	E/E
PIVVUO	Ph	Cl^-	E/E
RABKAJ	^{t}Bu	Cl^-	E/E
RABKJA01	^{t}Bu	Cl^-	E/E
SOFBIB	^{i}Pr	Cl^-	E/Z
TOCBAQ	^{t}Bu	GeF_3^-	E/E
TOCBEU	^{t}Bu	$Sn_2F_6^{2-}$	E/E
ULIPAI	^{i}Pr	benzene-1,2-dicarboxylate	E/Z
ULIPEM	^{i}Pr	benzene-1,3-dicarboxylate	E/Z
ULIPIQ	^{i}Pr	2,6-naphthalenedisulfonate	E/Z
ULIPOW	^{i}Pr	1,5-naphthalenedisulfonate	E/Z
UWIHOZ	Ph	NO_3^-	Z/Z
XOMJUH	Et	Cl^-	E/Z
XONFEP	4-CF_3Ph	Br^-	Z/Z
XONFOZ	4-CF_3Ph	Br^-	Z/Z
YEBZOV	MeBn	2,4,6-triphenylbenzoate	E/E
YUQSIN	Ph	fumarate	E/E

[a] CSD codes POJRUF and REJVAH were discounted because they contained P or Si atoms coordinated to the amidinium group.

4.3 Angle between amidinium and phenyl group search parameters

The Cambridge Structural Database[11] (CSD) Version 6.00 (April 2025) was searched for substituted benzamidinium groups as described in Section 4.1. We then measured the mean plane angle between the plane defined by the six carbon atoms of the phenyl ring, and the two nitrogen atoms and two carbon atoms of the amidinium group (*i.e.* the two nitrogen atoms, the carbon between them, and the ring carbon attached to this).

As shown in Table S8, there are only four dimethylbenzamidinium and five diethylbenzamidinium structures in the CSD. We therefore also included the 15 dimethylamidinium structures that we reported recently (not yet in the CSD),[2] and the five diethylamidinium structures reported in this work to obtain a more meaningful number of datapoints.

4.4 Angle between amidinium and phenyl group search results

As shown in Table S9, a wide range of angles are seen between amidinium and phenyl groups, however it is clear that on average diethylamidinium groups have larger angles with their phenyl substituents (68°) than do dimethylbenzamidiniums (59°). Both of these values are far higher than those for unsubstituted benzamidinium groups (33°). It is notable that values approaching 0° (*i.e.* a co-planar arrangement of the phenyl and amidinium groups), but the lowest mean plane angle observed for dimethylbenzamidinium groups is 44° and for diethylbenzamidiniums is 47°.

Table S9. X-ray crystal structures of alkyl- and aryl-substituted benzamidiniums in the CSD, reported in Reference [2] and in this work.

	Unsubstituted benzamidinium	**Dimethylbenzamidinium**	**Diethylbenzamidinium**
Number of angles	577	37	19
Minimum angle (°)	0.8	43.7	47.1
Maximum angle (°)	89.8	88.6	88.2
Median angle (°)	31.9	57.3	71.5
Mean angle (°)	32.8	59.1	68.2
ESD of mean[a] (°)	0.6	1.8	2.5
95% confidence interval of mean (°)	31.6 – 34.0	55.5 – 62.7	63.2 – 73.2

[a] Estimated as ESD = s/√n where s is the sample standard deviation and n is the number of values.

5 Density functional theory calculations

5.1 General remarks

5.1.1 Methodology

Density functional theory calculations were conducted on the cationic compounds and conformations shown in Figure S38. These calculations were conducted in Spartan24[12] using either ωB97X-D[13] or M06-2X[14] functionals and the 6-311G+** basis set. Calculations were conducted in both the gas phase and in implicit water using the C-PCM model[15] within Spartan24.[12] We emphasise that the use of an implicit solvent model is a relatively simplistic treatment of solvent effects, but these calculations were conducted as a crude measure of the effect of solvation.

5.1.2 Starting geometries

CSD searches (Section 4) revealed that *Z/Z* conformations have only been observed in the solid state when aryl groups are directly attached to the amidinium nitrogen atom. Given the major focus of these studies was on dimethylamidiniums and diethylamidiniums, we only calculated energies for the *E/E* and *E/Z* conformations and not the *Z/Z* conformations, although we acknowledge that this conformation may be significant for **^{Ph}calc$^+$**.

For ***E,Z*-^{Me}calc$^+$**, the X-ray crystal structure of **^{Me}model·BPh$_4$**[2] was modified to remove the anion and 4-*tert*-butyl group. An equilibrium geometry calculation was then carried using the M06-2X functional and 6-31+G* basis set in the gas phase, with a 1+ charge. Subsequently, DFT equilibrium geometry and energy calculations were conducted using the parameters summarised in Table S9. For ***E,E*-^{Me}calc$^+$**, the CSD entry AQEVAT was manually edited by deleting the anion, the 4-ethyl group on the phenyl ring, and truncating the *N*-ethyl groups to methyl groups, and then conducting equilibrium geometry and energy calculations using the parameters summarised in Table S9.

For ***E,Z*-^{Et}calc$^+$**, the X-ray crystal structure of **^{Et}biphen·Cl$_2$** (Section 3) was modified to delete the anions, solvents, and one of the phenyl diethylamidinium groups. An equilibrium geometry calculation was then carried out at the semi-empirical PM6[16] level of theory in the gas phase, with a 1+ charge. Subsequently, DFT equilibrium geometry and energy calculations were conducted using the parameters summarised in Table S9. For ***E,E*-^{Et}calc$^+$**, the CSD entry AQEVAT was manually edited to remove the anion and 4-ethyl group on the phenyl ring; one of the ethyl groups in this crystal structure is in an unusual arrangement (presumably due to crystal packing effects), which caused issues with calculations and so this was manually moved to have a similar geometry to the other ethyl group. Semi-empirical and DFT calculations were then conducted as described for ***E,E*-^{Et}calc$^+$**.

For ***E,Z*-^{iPr}calc$^+$**, the CSD entry ULIPAI was modified to delete the anion and additional functionality. An equilibrium geometry calculation was then carried out at the semi-empirical PM6[16] level of theory in the gas phase, with a 1+ charge. Subsequently, DFT equilibrium geometry and energy calculations were conducted using the parameters summarised in Table S9. For ***E,E*-^{iPr}calc$^+$**, the CSD entry ARITIG was modified to delete the anion. An equilibrium geometry calculation was then carried out at the semi-empirical PM6[16] level of theory in the gas phase, with a 1+ charge. Subsequently, DFT equilibrium geometry and energy calculations were conducted using the parameters summarised in Table S9.

For ***E,E*-^{Ph}calc$^+$**, the CSD entry YUQSIN was modified to delete the anion. An equilibrium geometry calculation was then carried out at the semi-empirical PM6[16] level of theory in the gas phase, with a 1+ charge. Subsequently, DFT equilibrium geometry and energy calculations were conducted using the parameters summarised in Table S9. For ***E,Z*-^{Ph}calc$^+$**, the CSD entry YUQSIN was manually edited by replacing one hydrogen atom with a phenyl group and one phenyl group with a hydrogen atom, and then conducting semi-empirical and DFT calculations as described for ***E,E*-^{Ph}calc$^+$**.

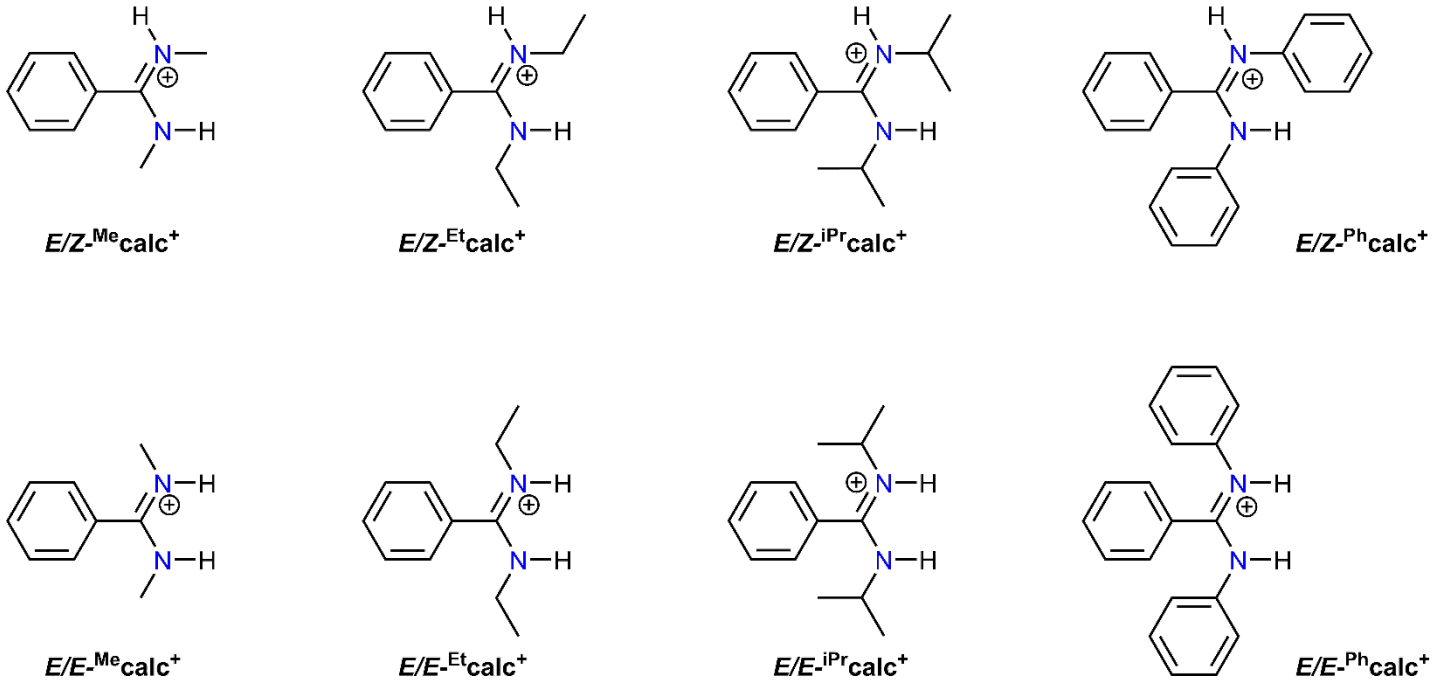

Figure S38. Structures and conformations of compounds studied by DFT calculations.

5.2 Calculated structures

DFT-optimised gas phase structures for the eight compounds/conformers are shown in Figure S39. These structures, and those calculated using the ωB97X-D functional and for both M06-2X and ωB97X-D in implicit water are provided in .xyz format as Electronic Supplementary Information.

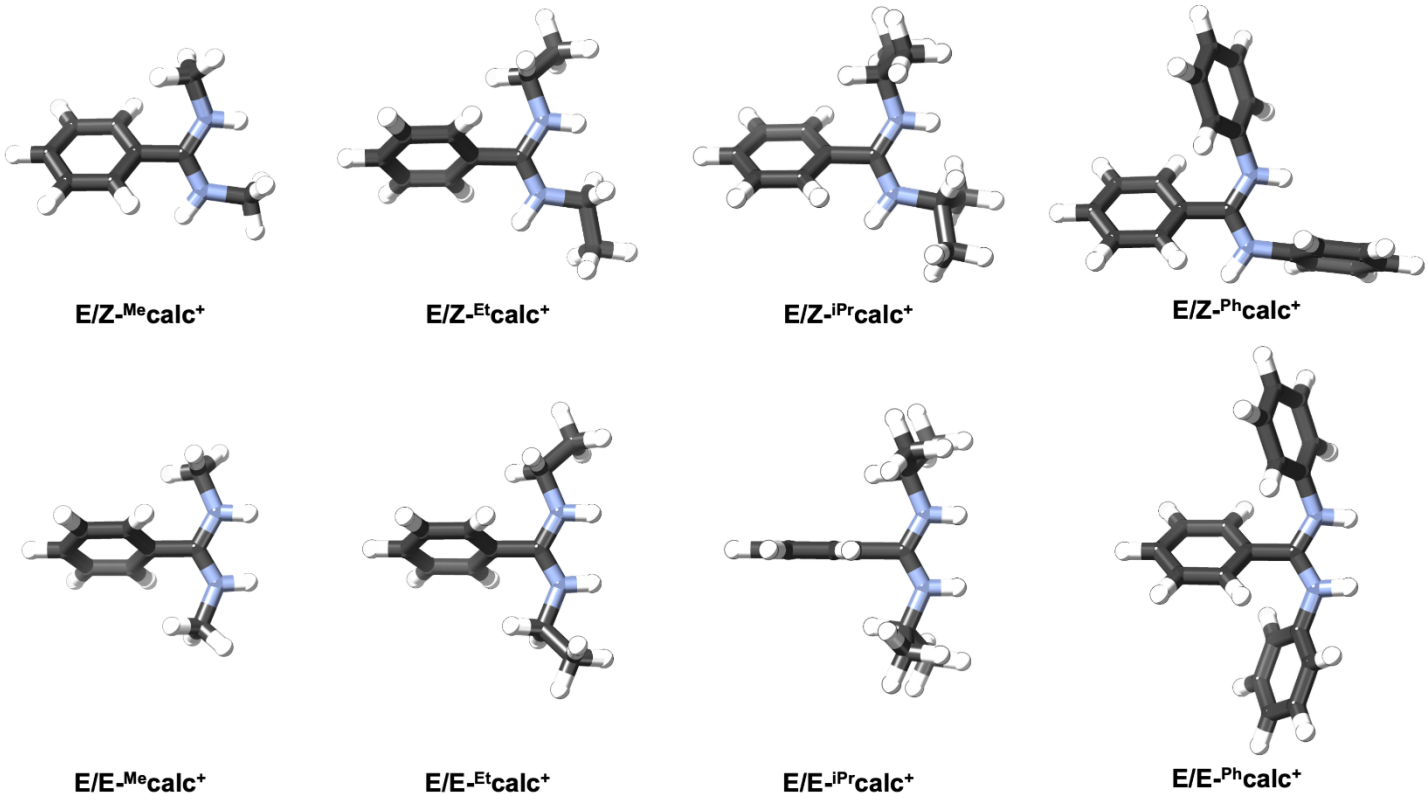

Figure S39. DFT-optimised gas phase structures of compounds using the M06-2X functional and 6-311G+** basis set. Calculated structures in implicit water, or using the ωB97X-D functional are provided in .xyz format as Electronic Supplementary Information.

5.3 Energy differences between conformers

As shown in Table S10, for all studied systems, the *E/Z* conformation was calculated to be more favourable than the *E/E* conformation (consistent with solution NMR studies, Section 2). For the methyl and ethyl-substituted amidiniums, the energy difference is 12 – 13 kJ mol^{-1} in the gas phase and 8 – 10 kJ mol^{-1} in implicit water. For the isopropyl-substituted amidiniums, the gap is slightly smaller in both the gas phase (10 – 12 kJ mol^{-1}) and in implicit water (4 – 6 kJ mol^{-1}); these values in implicit water are similar to that calculated by Grosu and Legrand for the same molecule using a different functional, basis set and solvation model (5.4 kJ mol^{-1}).[17] For the phenyl-substituted amidiniums, the energy gap is larger in the gas phase (16 – 17 kJ mol^{-1}) but small in implicit water (~ 2 kJ mol^{-1}).

Table S10. Calculated energy differences between *E/Z* and *E/E* conformations of various substituted amidinium compounds.

Compound	Functional	Solvent	Favourability of *E/Z* conformation (kJ mol^{-1})
^{Me}calc$^+$	ωB97X-D	gas	12.3
^{Me}calc$^+$	M06-2X	gas	13.0
^{Me}calc$^+$	ωB97X-D	water[a]	8.7
^{Me}calc$^+$	M06-2X	water[a]	9.8
^{Et}calc$^+$	ωB97X-D	gas	12.5
^{Et}calc$^+$	M06-2X	gas	13.2
^{Et}calc$^+$	ωB97X-D	water[a]	8.3
^{Et}calc$^+$	M06-2X	water[a]	9.3
^{iPr}calc$^+$	ωB97X-D	gas	9.7
^{iPr}calc$^+$	M06-2X	gas	11.8
^{iPr}calc$^+$	ωB97X-D	water[a]	3.8
^{iPr}calc$^+$	M06-2X	water[a]	6.0
^{Ph}calc$^+$	ωB97X-D	gas	17.1
^{Ph}calc$^+$	M06-2X	gas	16.4
^{Ph}calc$^+$	ωB97X-D	water[a]	2.0
^{Ph}calc$^+$	M06-2X	water[a]	2.4

[a] Implicit water simulated using a C-PCM model.[15]

6 References

[1] H. E. Gottlieb, V. Kotlyar, A. Nudelman, NMR Chemical Shifts of Common Laboratory Solvents as Trace Impurities", *J. Org. Chem.* **1997**, *62*, 7512–7515.

[2] M. K. S. Perry-Britton, N. G. White, Hydrogen-Bonded Networks from Poly(dimethylamidinium) Cations and Polycarboxylate Anions, *Cryst. Growth Des.* **2025**, *25*, 9876–9885.

[3] *Bindfit*, accessed at supramolecular.org.

[4] *CrysAlisPro*, Oxford Diffraction, UK, **2011**.

[5] L. Palatinus, G. Chapuis, SUPERFLIP. A computer program for the solution of crystal structures by charge flipping in arbitrary dimensions, *J. Appl. Crystallogr.* **2007**, *40*, 786–790.

[6] G. Sheldrick, SHELXT - Integrated space-group and crystal-structure determination, *Acta Crystallogr.* **2015**, *A71*, 3–8.

[7] P. W. Betteridge, J. R. Carruthers, R. I. Cooper, K. Prout, D. J. Watkin, CRYSTALS version 12: software for guided crystal structure analysis, *J. Appl. Crystallogr.* **2003**, *36*, 1487.

[8] A. L. Spek, PLATON SQUEEZE: a tool for the calculation of the disordered solvent contribution to the calculated structure factors, *Acta Crystallogr.* **2015**, *C71*, 9–18.

[9] R. I. Cooper, A. L. Thompson, D. J. Watkin, CRYSTALS enhancements: dealing with hydrogen atoms in refinement, *J. Appl. Crystallogr.* **2010**, *43*, 1100–1107.

[10] D. Aragao, J. Aishima, H. Cherukuvada, R. Clarken, M. Clift, N. P. Cowieson, D. J. Ericsson, C. L. Gee, S. Macedo, N. Mudie, S. Panjikar, J. R. Price, A. Riboldi-Tunnicliffe, R. Rostan, R. Williamson, T. T. Caradoc-Davies, MX2: a high-flux undulator microfocus beamline serving both the chemical and macromolecular crystallography communities at the Australian Synchrotron, *J. Synchrotron Radiat.* **2018**, *25*, 885–891.

[11] R. Taylor, P. A. Wood, "A Million Crystal Structures: The Whole Is Greater than the Sum of Its Parts" *Chem. Rev.* **2019**, *119*, 9427–9477.

[12] *Spartan24*, Wavefunction Inc., USA, **2025**.

[13] J.-D. Chai, M. Head-Gordon, Long-range corrected hybrid density functionals with damped atom–atom dispersion corrections, *Phys. Chem. Chem. Phys.* **2008**, *10*, 6615.

[14] Y. Zhao, D. G. Truhlar, The M06 suite of density functionals for main group thermochemistry, thermochemical kinetics, noncovalent interactions, excited states, and transition elements: two new functionals and systematic testing of four M06-class functionals and 12 other functionals, *Theor. Chem. Acc.* **2008**, *120*, 215–241.

[15] M. Cossi, N. Rega, G. Scalmani, V. Barone, Energies, structures, and electronic properties of molecules in solution with the C-PCM solvation model, *J. Comput. Chem.* **2003**, *24*, 669–681.

[16] J. J. P. Stewart, Optimization of parameters for semiempirical methods V: Modification of NDDO approximations and application to 70 elements, *J. Mol. Model.* **2007**, *13*, 1173–1213.

[17] L. Pop, N. D. Hadade, A. van der Lee, M. Barboiu, I. Grosu, Y.-M. Legrand, Occurence of Charge-Assisted Hydrogen Bonding in Bis-amidine Complexes Generating Macrocycles, *Cryst. Growth Des.* **2016**, *16*, 3271–3278.